A PRECIPITATION-BASED UNIVERSAL DETECTION PLATFORM FOR DNA AMPLIFICATION REACTION USING BOVINE SERUM ALBUMIN-MODIFIED GOLD NANOPARTICLES AND REDUCED GRAPHENE OXIDE

WANG SHIYAO

M.Phil

The Hong Kong Polytechnic University

2018

The Hong Kong Polytechnic University
Department of Biomedical Engineering

A Precipitation-Based Universal Detection Platform for DNA Amplification Reaction Using Bovine Serum Albumin-Modified Gold Nanoparticles and Reduced Graphene Oxide

WANG Shiyao

A thesis submitted in partial fulfillment of the requirements
for the degree of Master of Philosophy
October 2017

CERTIFICATE OF ORIGINALITY

I hereby declare that this thesis is my own work and that, to the best of my knowledge and belief, it reproduces no material previously published or written, nor material that has been accepted for the award of any other degree or diploma, except where due acknowledgement has been made in the text.

_____ (Signed)

WANG Shiyao (Name of student)

Abstract

The detection of nucleic acid plays an increasingly significant role in various fields, including medical diagnosis, food safety testing, and biowarfare agent detection. The gold standard technique is real-time polymerase chain reaction, which involves fluorescent signal readout. Due to the use of the complicated and expensive instrument, these assays are performed in central laboratories. Toward decentralized testing (point-of-care/field testing), which can provide timely treatment/response decision, a simple signal readout is essential. Gold nanoparticles (AuNPs) have been intensively investigated for DNA detection by virtue of their result readout by the naked eye. Typically, these assays involve the use of two sets of oligonucleotide-modified gold nanoparticles (oligo-AuNPs) (each being complementary to half of a target sequence), by which target recognition and signal readout are coupled. In the absence of the target, oligo-AuNPs are dispersed and the solution appears red in color, while in the presence of the target, oligo-AuNPs are cross-linked/aggregated and the solution turns purple. However, it should be noted that oligo-AuNPs are prepared using thiol-modified oligonucleotides, which is expensive. Besides, the red-to-purple color change can sometimes be difficult to differentiate by the naked eye. In this thesis, a new type of AuNPs (bovine serum albumin-modified AuNPs, BSA-AuNPs; responsible for signal readout) together with reduced graphene oxide (rGO; responsible for target recognition) are utilized for the detection of a target DNA sequence based on the precipitation-based readout. In the absence of the target, single-stranded oligonucleotide probe binds with rGO via π-stacking

interaction and stabilizes rGO from salt-induced aggregation. Upon the addition of BSA-AuNPs, a red dispersion is obtained. While in the presence of the target, the double-stranded probe-target hybrid does not bind with rGO. Upon the addition of salt followed by BSA-AuNPs, a red precipitate is obtained (co-precipitation of BSA-AuNPs with the aggregated rGO). The limit of detection for oligonucleotide target was 5 nM. Moreover, this assay scheme is readily applicable to polymerase chain reaction (PCR) and helicase-dependent amplification (HDA) product detection, thereby achieving the limits of detection of 83 fM and 21 aM, respectively. Taken together, this new assay platform has the advantages of facile and low-cost preparation (BSA-AuNPs versus oligo-AuNPs), simple result readout, and ultrasensitive detection. It is well suited for decentralized testing and, to the best of our knowledge, is the first attempt of utilizing the co-precipitation of BSA-AuNPs with rGO for nucleic acid detection.

List of Publication

1. Wang, S.Y., Chau, L.Y., Qin, A.L., He, Q.J., Yip, S.P., Lee, T.M.H., A Precipitation-Based Universal Detection Platform for DNA Amplification Reaction Using Bovine Serum Albumin-Modified Gold Nanoparticles and Reduced Graphene Oxide, in preparation.

Acknowledgements

I would like to express my gratitude to my supervisor, Dr. Thomas Lee, for his guidance and encouragement throughout my study. I would also like to thank my co-supervisor Prof. S. P. Yip for the great support in the PCR and HDA experiments. Also, I want to thank my colleagues in S106b, Dr. Li Yin Chau, Ms. Qijin He, Ms. Ailin Qin, and Ms. Maria Gan for their stimulating discussions and for the days we were working together. Last but not least, I would like to thank my family for their unconditional love, understanding, and support throughout my life.

Table of Contents

List of Figures

List of Abbreviations

AuNPs	gold nanoparticles
AHPND	acute hepatopancreatic necrosis disease
BSA	bovine serum albumin
BSA-AuNPs	bovine serum albumin-modified gold nanoparticles
DNA	deoxyribonucleic acid
dNTP	deoxyribonucleoside triphosphate
ddNTPs	dideoxynucleotides
DLS	dynamic light scattering
dsDNA	double-stranded DNA
ELISA	enzyme-linked immunosorbent assay
FRET	fluorescence resonance energy transfer
FTIR	Fourier transform infrared spectroscopy
GO	graphene oxide
HDA	Helicase-dependent amplification
H_2SO_4	sulfuric acid
ICAN	isothermal and chimeric primer-initiated amplification of nucleic acids
IEP	isoelectric point
$KMnO_4$	potassium permanganate
LAMP	loop-mediated isothermal amplification
LSPR	localized surface plasmon resonance
MB	molecular beacon
MiRNA	microRNA
NASBA	nucleic acid sequence based amplification
$NaNO_3$	sodium nitrate
oligo-AuNPs	oligonucleotide-modified gold nanoparticles

PCR	polymerase chain reaction
POC	point-of-care
PNA	peptide nucleic acid
RNA	ribonucleic acid
rGO	reduced graphene oxide
RCA	rolling circle amplification
ssDNA	single-stranded DNA
SDA	strand displacement polymerase amplification
Tris	tris(hydroxymethyl)aminomethane
TEM	transmission electron microscopy
UltraPure water	UltraPure DNase/RNase-free distilled water
WSSV	white spot syndrome virus

Chapter 1 Introduction

The detection of biomolecules plays an increasingly critical role in various fields in recent years, including medical diagnosis, environmental monitoring, food safety testing, and biowarfare agent detection. Nucleic acids consist of deoxyribonucleic acid (DNA) and ribonucleic acid (RNA). Conventional detection methods for nucleic acids are time-consuming and require complex procedures, experienced operators, and expensive instruments, which shows inefficient disease control and is not suitable for resource-limited regions. Therefore, there is a great need for point-of-care or on-site testing featuring rapid, simple, and cost-effective detection platforms for nucleic acid [1].

In recent years, a great number of nucleic acid assay platforms has been developed. Most of these systems achieve improved detection performance by using nanomaterials due to their unique optical, electronic, chemical, and catalytic properties, such as gold nanoparticles (AuNPs) and graphene-based materials including graphene, graphene oxide (GO) and reduced graphene oxide (rGO). Signal generated from these platforms can be detected by fluorescence/ultraviolet/visible spectrophotometer, electrical sensor, digital camera, smartphone or the naked eye, depending on the property of the used nanomaterials and the mechanism of detection. It should be noted that, in most of these nanomaterial-based detection platforms, a high concentration of the target (nanomolar level) is needed to affect a detectable signal. As the amount of a target DNA/RNA sequence in real

samples is typically at femtomolar (or down to attomolar), which is too minute for direct detection, enzymatic amplification is commonly used to produce million to trillion copies of the target. Amplification and detection are the two essential elements of standard nucleic acid testing procedures to obtain a sensitive detection platform.

In this chapter, the amplification reactions for nucleic acid are summarized in Section 1.1. The research progress of AuNP-based nucleic acid detection platforms is presented in Section 1.2. The research progress of detection platforms for nucleic acid using graphene-based nanomaterials is described in Section 1.3. The challenges and limitations of current detection platforms are discussed in Section 1.4. Last, the objectives of this study are presented in Section 1.5.

1.1. Nucleic Acids Amplification

Considering that the target concentration in real samples is usually down to femtomolar or attomolar level, amplification process is necessary to be combined with detection part to achieve an effective platform with high sensitivity. The amplification methods can be classified as thermal cycling (need complex temperature control) or isothermal cycling (amplification can be carried out at a constant temperature).

1.1.1. Polymerase Chain Reaction (PCR)

Polymerase chain reaction (PCR), originally developed by Mullis and co-workers [2] is the most widely used thermal-cycling method to amplify a small amount of DNA, which involves repeated heating and cooling process. The components for typical PCR are DNA template, a pair of specifically designed primers, deoxyribonucleoside triphosphate (dNTPs), reaction buffer containing necessary ions for polymerase functioning, and thermostable DNA polymerase (eg., *Taq* polymerase). There are 3 steps for PCR amplification (as shown in Figure 1.1). The first step is denaturation. The mixtures are incubated at around 94–98 °C for several seconds and the double-stranded template or amplicon dissociate into single-stranded strands. The second step is primer annealing. The temperature for the reaction is cooled to 55–70 °C and single-stranded primers bind to the complementary sequences of template or amplicon based on the Watson-Crick principle of base pairing. Last, the primer extension is carried out at around 68–72 °C (the temperature of this step depends on the property of DNA polymerase involved in the reaction; 68 °C is suitable for *Taq* polymerase). Thus, after a 35-cycle of these 3 steps, the target DNA can be amplified from a single copy to billion copies in an exponential way, showing the great potential to be combined to achieve sensitive detection platforms for nucleic acid [3]. PCR contains excellent sensitivity and specificity, and reactions components for PCR are easy to obtain commercially, which makes it the most common amplification reactions at present. However, PCR is time-consuming compared with some isothermal reactions and difficult to be used in resource-limited regions and to reach a low cost because of the requirement of expensive thermal cyclers. These

disadvantages hinder the wider applications of PCR to some extent. At present, the recognition of PCR product in clinical laboratories is mainly based on the real-time fluorescence detection [4] by SYBR Green [5] and TaqMan probe [6].

Figure 1.1. Schematic illustration of the thermal cycling process in polymerase chain reaction (PCR) (adapted from [2]).

1.1.2. Isothermal Nucleic Acid Amplification Reactions

While thermal amplification needs complicated temperature control, isothermal amplification can be conducted at a constant temperature, showing the significant potential to be utilized in point-of-care detection which requires easy temperature control, such as water bath or hand warmer, and low cost (does not need an expensive thermal cycler). The reaction temperatures vary in different isothermal reactions. Higher temperatures correspond to the reaction kinetics and the stringency of

the amplification reaction [7]. The higher temperature is also able to positively affect the specificity of the reaction [8] by reducing nonspecific primer annealing.

1.1.2.1. Loop-Mediated Isothermal Amplification

Loop-mediated isothermal amplification (LAMP), invented by Notomi and co-workers [9], can be carried out at a constant temperature of 65 °C. The scheme of the LAMP is shown in Figure 1.2. Typically, it requires 4 or 6 different primers to identify 6 distinct regions on the target gene, which imparts high specificity. Bst enzyme, with strand displacement activity, is typically utilized in LAMP reactions. First, LAMP is initiated by the extension of a pair of inner primers. Then, the extended product is replaced by the elongation of outer primers. Due to the overhang sequence of inner primers, which is complementary to an adjacent region, the extended product folds into a stem-loop structure that serves as a new template for inner primers, while extending itself at the 3' end to generate additional recognition regions for remaining primers. An extra pair of loop primers can further accelerate the reaction. Subsequently, amplicons with various lengths can be produced. Hence, target sequences can be amplified exponentially in LAMP. Compared with PCR, LAMP has the advantages of high sensitivity, efficiency, and specificity. Besides, it does not require a thermal cycler, suitable to be applied in simple detection platforms.

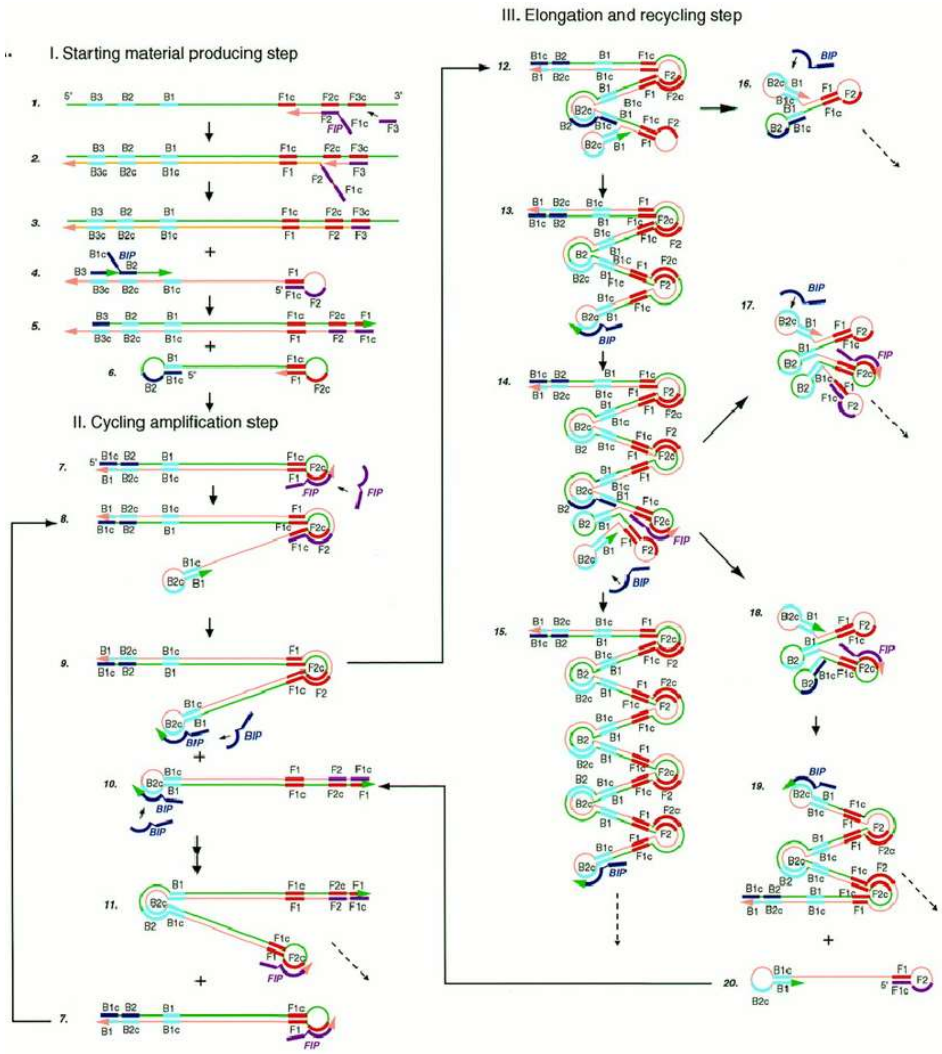

Figure 1.2. Schematic illustration of loop-mediated isothermal amplification (LAMP) (adapted from [9]).

1.1.2.2. Helicase-Dependent Amplification

Helicase-dependent amplification (HDA), invented by Vincent and co-workers [10], is an isothermal amplification method, utilizing a DNA helicase to generate single-stranded templates instead of the high temperature in PCR. There is a pair of primers needed to recognize the specific region of templates. The scheme of HDA is shown in Figure 1.3.

Firstly, helicase unwinds the double-stranded templates to single-stranded structure. Secondly, designed primers bind to the single strands of templates via base pairing principle. Thirdly, DNA polymerase is used to extend the primers, and each duplex can be amplified to two duplexes. These three steps are recycling due to the unwinding of newly produced duplexes by the helicase. Hence, the target sequences can be amplified in an exponential way. The typical temperature of HDA is around 65 °C and the lowest target amount to initialize HDA reaction is only one copy, showing the significant potential for the applications in simple and sensitive detection platforms.

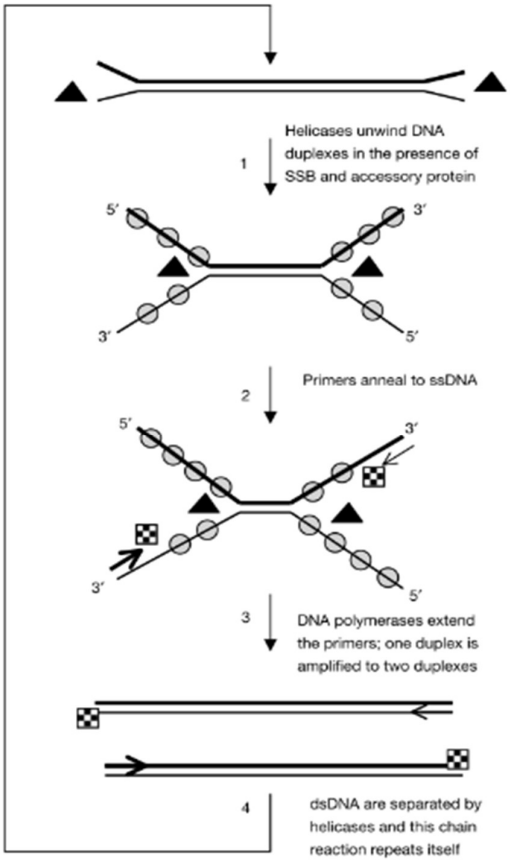

Figure 1.3. Schematic illustration of the helicase-dependent amplification (HDA) (adapted from [10]).

Apart from the amplification reactions mentioned above, there are many other kinds of isothermal amplification platforms for nucleic acids. Their mechanisms are various in terms of reaction temperature, amount of primers required, and type of template (DNA or RNA). For example, nucleic acid sequence based amplification (NASBA) [11] is an isothermal amplification method for RNA template with high sensitivity. In addition, Isothermal and chimeric primer-initiated amplification of nucleic acids (ICAN) [12] can achieve efficient amplification of target DNA at around 55 °C (with an initial temperature at 95 °C for template denaturation) using only one pair of chimeric primers.

1.2. AuNPs for Nucleic Acid Detection

1.2.1. AuNPs and Their Optical Properties

Nanomaterials have the unique advantages of ultrasmall size (1–100 nm), large surface area-to-mass ratio, and high reactivity, hence possessing the potential to overcome the limitations of traditional diagnostics and therapeutics [13]. To date, there are a lot of platforms using nanomaterials for nucleic acid detection. AuNPs are the most stable metal nanoparticles, showing the properties which are different from both small molecules and bulk material, as well as from other kinds of nanoparticles [14]. They have attracted considerable attention due to the behavior of the individual particles, size-related electronic, magnetic, and optical properties [15].

There are many methods available for synthesizing AuNPs with specific sizes (varies from 1 to 150 nm). The most popular synthesis method was firstly reported by Turkevich and co-workers [16] in 1951. They used

citrate reduction method to synthesize gold nanoparticles from $HAuCl_4$ in water. The scheme of this reaction is shown in Figure 1.4. In this method, sodium citrate serves as both reducing agent and capping agent. The size of synthesized AuNPs using this method is typically 13 nm in diameter.

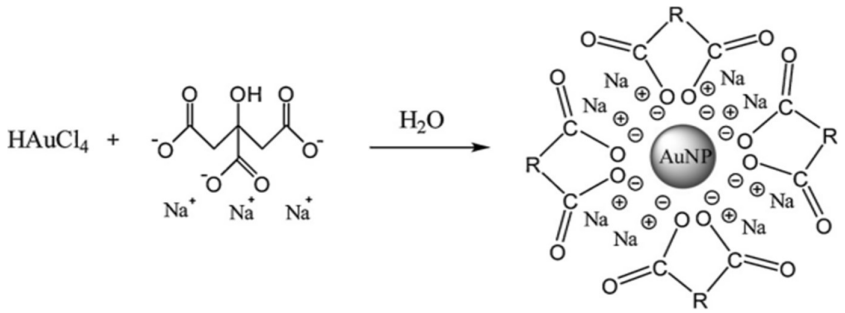

Figure 1.4. AuNP synthesis using the citrate reduction method (adapted from [16]).

The unique physical properties of AuNPs, especially the optical properties, make AuNPs attractive signal transducer or signal amplifier in various colorimetric detection platforms [17]. It is well-known that bulk gold is gold in color. However, gold nanoparticles can show various colors such as red, purple, blue, or green, due to the interaction of conduction band electrons in the metallic nanoparticles with the electric field vector of the incident light. This interaction is called the localized surface plasmon resonance (LSPR), which occurs in the visible and near-infrared regime of the spectrum for AuNPs, depending on their shape, size, and interparticle distance [18]. The size-dependent optical property is shown in Figure 1.5 (top). The colors of AuNPs solutions with varied sizes are various. The interparticle distance-dependent optical property is shown in Figure 1.5 (bottom). When visible light shines on AuNPs, the light of a resonant wavelength is absorbed by AuNPs and

induces surface electron oscillation. Small dispersed AuNPs (13 nm in diameter) absorb green light, which corresponds to a strong absorption band (surface plasmon band) at around 520 nm in the visible light spectrum, thus appear red in color. The aggregation of AuNPs corresponds to a red-to-purple color change of the solution, which is easy to read out by the naked eye. This unique optical property has been widely used for the detection of biomolecules in the recent decade.

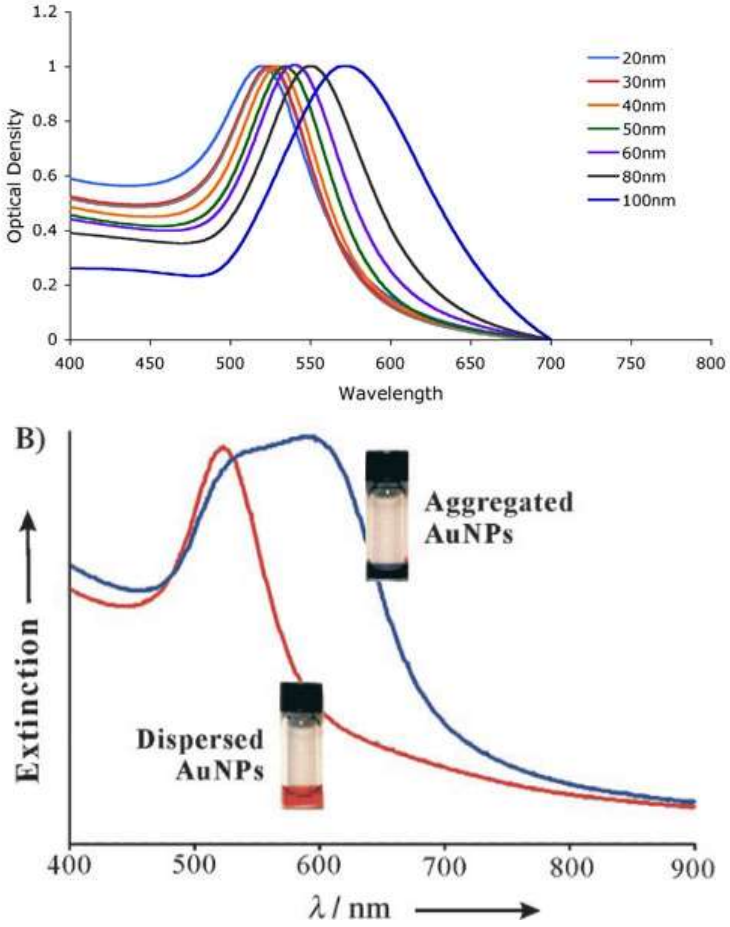

Figure 1.5. (Top) Size-dependent optical property of AuNPs (adapted from [19]). (Bottom) Interparticle distance-dependent surface plasmon absorption bands for 13 nm AuNPs. The red and blue curves correspond to dispersed and aggregated AuNPs, respectively (adapted from [17]).

1.2.2. Functionalization of AuNPs

Functionalization of gold nanoparticles significantly improves the potential of gold nanoparticles in biomedical applications. In recent years, there has been a rich variety of functional molecular linkers and passivating agents employed in the conjugation of gold nanoparticles. The types of facile functionalization of gold nanoparticles include thiolate, citrate, amine, carboxylate, nucleic acid, peptide, antibody, and lipid ligands. Citrate is the most common electrostatic stabilizing agent for gold nanoparticles due to the typical synthesis of gold nanoparticles using sodium citrate reduction method. Citrate-modified gold nanoparticles are susceptible to environmentally induced aggregation, so they are commonly the important precursors of covalent conjugates with additional functionality.

1.2.2.1. Oligonucleotide-Modified Gold Nanoparticles (Oligo-AuNPs)

Mirkin and co-workers have pioneered the use oligo-AuNPs [20]. The oligo-AuNPs were prepared by mixing alkanethiol-terminated oligonucleotides and citrate-modified AuNPs. Oligonucleotide ligands first displace the citrate from the AuNPs through the formation of a gold-thiol bond. Then, NaCl was added to the reaction mixture to shield charge repulsion, thus allowing a greater number of oligonucleotides to chemically adsorb to the nanoparticle surface, resulting in a dense monolayer of oligonucleotides (shown in Figure 1.6) [21]. Currently, most of the AuNP-based nucleic acid platforms involve the use of oligo-AuNPs, however, which means expensive and complicated preparation procedures.

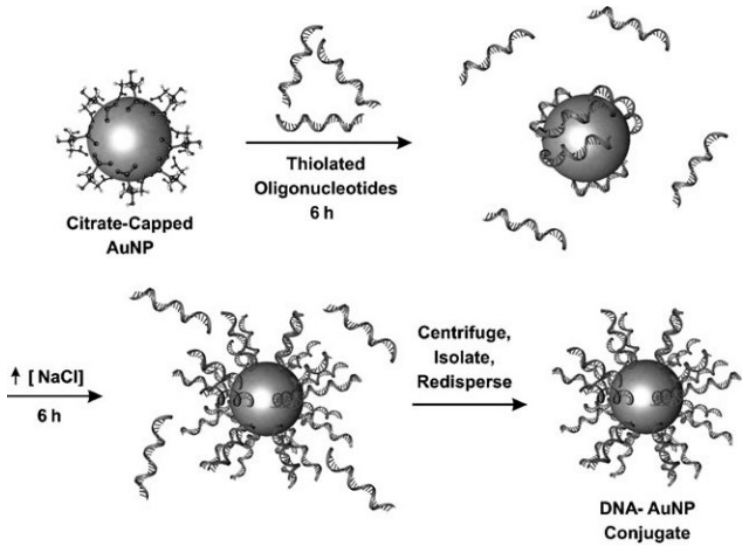

Figure 1.6. Schematic illustration of preparation of oligonucleotide-modified AuNPs (oligo-AuNPs) (adapted from [21]).

1.2.2.2. Bovine Serum Albumin-Modified Gold Nanoparticles (BSA-AuNPs)

Apart from nucleic acids, protein is also widely used to functionalize gold nanoparticles. Protein is complex amphiphilic biopolymers with hydrophobic and hydrophilic patches on the surfaces, which indicates the adhesiveness to solid surfaces [22]. BSA is one of serum albumin proteins and plays a vital role in various bioanalytical applications as a blocking agent due to its high efficiency, cost-effectiveness, and great biocompatibility [23]. It can prevent the non-specific protein-protein interactions or protein-surface interactions in diverse biochemical experiments such as enzyme-linked immunosorbent assay (ELISA) [24]. The modification of BSA was commonly used for increasing the stability of AuNPs in detection platforms [25]. The binding of BSA to the surface of citrate-modified AuNP appeared to be a spontaneous process,

whereas the mechanism of the binding remained undetermined. In 2005, Franzen and co-workers reported that the binding of BSA to citrate-modified AuNPs was mainly due to the electrostatic mechanism consisting of salt bridges, while the results did not exclude contributions from steric or hydrophobic interactions [26]. Moreover, due to the spontaneous adsorption of BSA to the gold surface, BSA is commonly used as a sacrificial protein that competes with Taq DNA polymerase for adsorption onto the AuNP surface to increase the compatibility of AuNPs in PCR [27]. In 2014, Yang and co-workers demonstrated the preparation of BSA-AuNPs by simply adding BSA solution into the AuNPs synthesized by citrate reduction method, followed by subsequent stirring of the mixture for 20 hours at room temperature [28]. BSA-AuNPs have the advantages of relatively high stability, low cost, and ease of preparation, showing the significant potential in point-of-care (POC) detection. However, until now, there is no platform using BSA-AuNPs as detection reporters for nucleic acid detection.

1.2.3. AuNP-Based Nucleic Acid Detection

For nucleic acid detection, visual readout enabled by the unique interparticle distance-dependent optical property of AuNP probes has received considerable attention in recent years. Nowadays, there are three mechanisms commonly used for AuNP- based nucleic acid detection. The first detection mechanism involves two sets of oligo-AuNPs to bind target sequence in a sandwich configuration [20, 29, 30]. One platform reported by Mirkin and co-workers [29] used oligo-AuNPs as probes to detect the polynucleotide targets. The scheme is shown in Figure 1.7. The target-induce cross-linking of the AuNP probes resulted in a decrease in the interparticle distance and thus a red shift of the

surface plasmon absorption band, with a concomitant solution color change from red to purple. The decrease of the interparticle distance resulted in the color change of the samples, thus showing the presence of the polynucleotide targets. The limit of detection was determined to be around 1 nM.

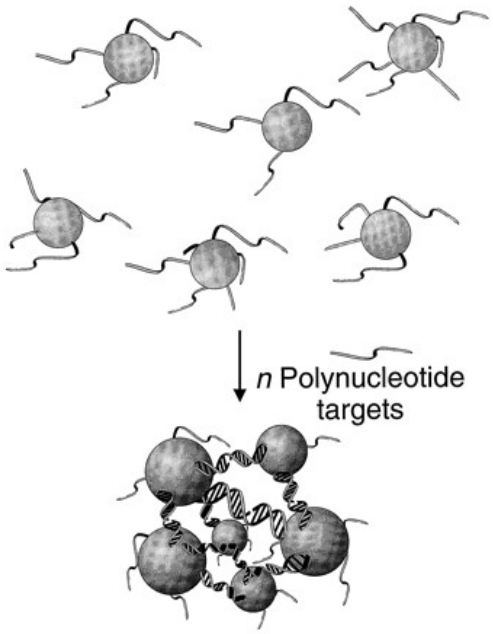

Figure 1.7. Schematic illustration of selective colorimetric detection of polynucleotides based on distance-dependent optical properties of AuNPs (adapted from [29]).

The second detection mechanism involves a single set of oligo-AuNPs (non-cross-linking) that unhybridized and hybridized probes have different stabilities against salt-induced aggregation [31, 32]. In 2003, Sato and co-workers [31] discovered an aggregation phenomenon of oligo-AuNPs induced by the hybridization of target DNA which did not cross-link the nanoparticles (Figure 1.8). They found that hybridized probes showed lower stability than unhybridized probes under specific salt concentration due to change of repulsive interaction between

particles. The aggregation of AuNPs induced by fully complementary target corresponded to a purple color while only probes or with mismatched targets appeared red, which was then applied to the detection of DNA. This detection method is considered to be rapid, simple, and specific and the limit of detection was nanomolar level.

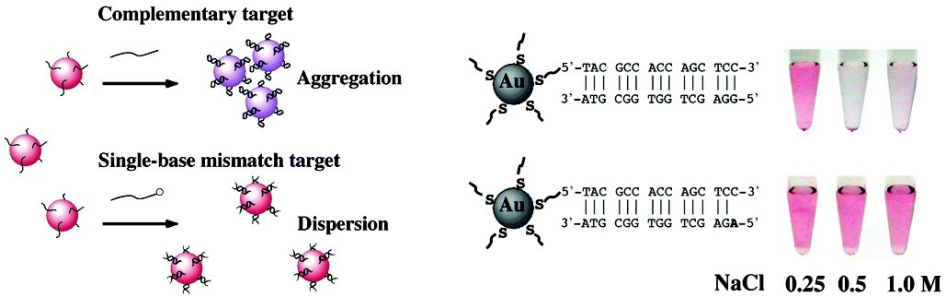

Figure 1.8. (Left) Schematic illustration of AuNP-based detection of DNA target using non-cross-linking mechanism. (Right) Fully complementary sequences led to different color compared with single-base mismatched sequences when salt concentration was higher than 0.5 M (adapted from [31]).

The third detection mechanism involves unmodified AuNPs that bind with single-stranded DNA and are stabilized against salt-induced aggregation but not with double-stranded hybrid (i.e., recognition sequence hybridized with target sequence). In 2004, Rothberg and co-workers reported a colorimetric detection scheme of DNA using unmodified gold nanoparticles depending on the electrostatic interactions [33]. The scheme of this detection platform is shown in Figure 1.9. They demonstrated that ssDNA and dsDNA had different propensities to adsorb on AuNPs because of their electrostatic properties, which led to different color after adding a determined amount of salt due to the interparticle-distance dependent optical property of

gold nanoparticles. Hence, the presence of target DNA resulted in red-to-purple color change. This assay was complete within 5 minutes, and the low to 100 femtomoles of target DNA can be observed directly without instrumentation. Besides, single-base mismatch can be detected using this platform.

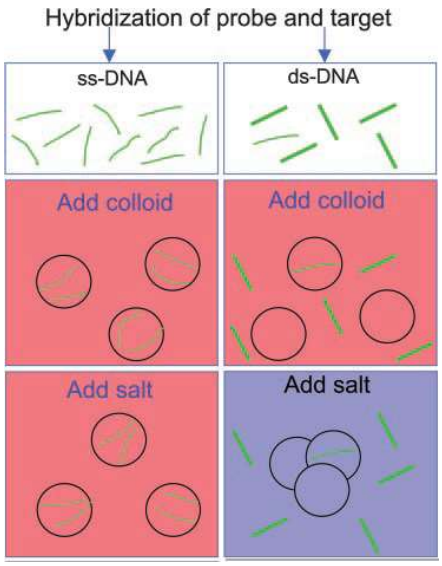

Figure 1.9. Schematic illustration of the colorimetric method for differentiating between single- and double-stranded oligonucleotides. The circles represent unmodified gold nanoparticles (adapted from [33]).

1.2.4. AuNP-Based Detection with Nucleic Acid Amplification

It is known that high concentration of target (nanomolar level) is commonly necessary to affect a detectable color change for visual detection. As the target in real samples is typically at femtomolar or down to attomolar level, significant efforts have been made to couple enzymatic amplification with AuNP-based detection, comprising both thermal-cycling and isothermal platforms. The combination with amplification can greatly improve the sensitivity of nucleic acid detection.

In 2005, Maeda and co-workers demonstrated a colorimetric detection platform for single-base substitutions in genomic DNA using oligonucleotide-modified AuNPs (Figure 1.10) [34]. This platform was combined with PCR. Firstly, DNA sequences containing target base were amplified by PCR, followed by the removal of excessive nucleotides. Next, the single-base extension was carried out with a typing primer and 4 kinds of dideoxynucleotides (ddNTPs). After the addition of probe-modified AuNPs and an appropriate amount of salt, samples containing mismatched base remained in red due to the dispersion of AuNPs. The work was considered as an innovative approach for simple and sensitive detection of single-nucleotide polymorphisms.

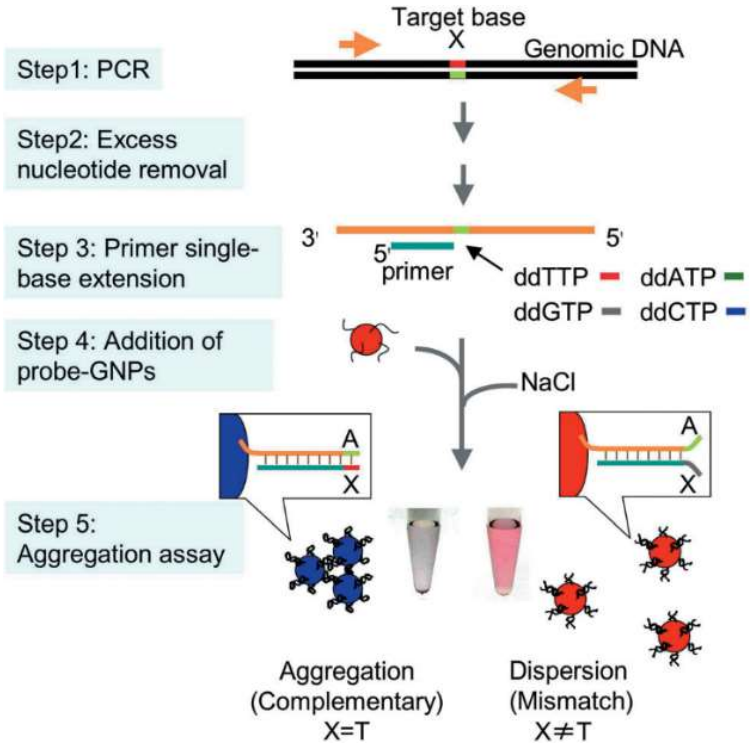

Figure 1.10. Schematic illustration of the platform combined with PCR using oligo-AuNPs for single-base substitutions detection (adapted from [34]).

Later in 2010, another AuNP-based nucleic acid detection platform coupled with PCR was reported by Park and co-workers (scheme is shown in Figure 1.11) [35]. Thiol-labeled primers were employed in this platform for the amplification of templates instead of typical unmodified primers. After successful PCR reaction of the target templates, each double-stranded product contained one thiol group at one end. Then unmodified AuNPs were added into the PCR products, followed by the addition of a critical amount of salt. The PCR products could strongly bind to the surface of AuNPs through the interaction of the terminal thiol groups, and the relatively long chain has sufficient negative charges which could subsequently lead to the stabilization of gold nanoparticles from salt-induced aggregation. Therefore, after PCR and addition of unmodified AuNPs and NaCl, the presence of target DNA could finally result in the maintenance of red color whereas the absence of target would lead to the red-to-purple color change of the solution.

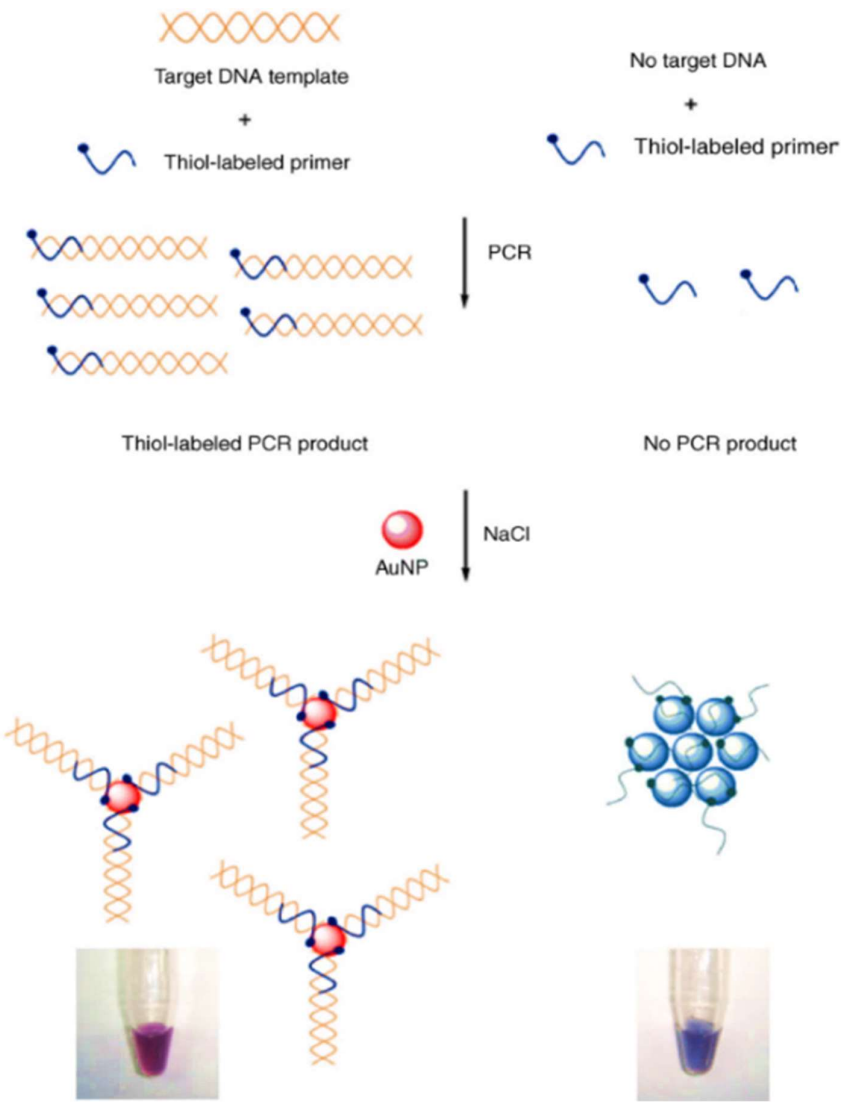

Figure 1.11. Schematic illustration of colorimetric detection utilizing thiol-labeled PCR primers and unmodified AuNPs (adapted from [35]).

More recently, Liang and co-workers demonstrated that gold nanoparticles combined with asymmetric PCR could be utilized for colorimetric DNA detection platform [36]. The overview of this work is shown in Figure 1.12. The specific DNA targets were firstly amplified by asymmetric PCR to generate single-stranded DNA (ssDNA) targets. Then after the addition of oligonucleotide-modified AuNPs, the bound oligo-probe on the surface of AuNPs selectively hybridized with the

complementary sequences of produced ssDNA targets, which led to self-assembly and aggregation of AuNPs and a corresponding red-to-purple occurred. The lowest limit to cause a detectable color change of this platform was picogram level, indicating the sensitivity was greatly improved compared with those platforms without the combination with nucleic acid amplification reactions.

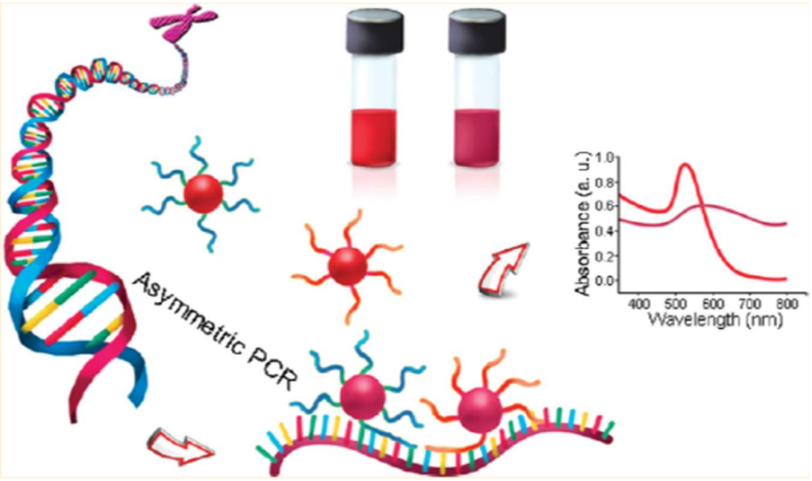

Figure 1.12. Overview of colorimetric detection of specific DNA with gold nanoparticles and asymmetric PCR (adapted from [36]).

Apart from the AuNP-based detection platforms with thermal amplification reactions, there are several isothermal amplification methods reported in AuNP-based nucleic acid detection. In 2008, Gill and co-workers coupled HDA with cross-linking detection scheme (shown in Figure 1.13) [37]. With HDA, the presence of a target sequence triggered the generation of amplicon in an exponential fashion. The amplicon sequence was designed to hybridize with two sets of oligo-AuNP probes. When the amplification reaction product was mixed with the oligo-AuNP probes, the positive sample (with the target) turned

purple whereas the negative sample (without the target) remained red.

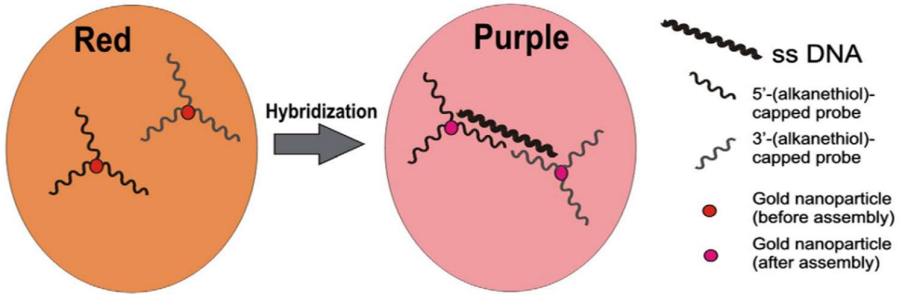

Figure 1.13. Schematic illustration of the detection through the hybridization of HDA product and oligo-AuNP probes (adapted from [37]).

Yet another isothermal platform with cross-linking detection mechanism was reported by Yang and co-worker in 2011 [38], in which exonuclease III was utilized to digest a reporter sequence when hybridized to a target sequence (limit of detection was 15 pM). There were several isothermal platforms with non-cross-linking detection mechanism [39–41]. In 2010, Li and co-workers reported that the EXPAR product of a positive sample stabilized oligo-AuNP probes (in this case only a single set of probes) against salt-induced aggregation. The same detection mechanism was applied to other isothermal amplification methods such as NASBA [40] and LAMP. In 2013, Kiatpathomchai and co-workers demonstrated a visual detection of white spot syndrome virus (WSSV) DNA using AuNPs with the LAMP [41]. The scheme is shown in Figure 1.14. Firstly, WSSV-specific probes were functionalized to AuNPs through thiol-metal interactions. Then, the probe-modified AuNPs were hybridized with the target DNA, followed by the addition of $MgSO_4$ as salt for effecting a color change. The sample containing target WSSV DNA retained red

while the sample in the absence of target turned to blue or gray due to the screening effect of salt. The sensitivity of this platform was determined to be approximately 0.03 μg per reaction of WSSV-LAMP generated product. More recently, the identical mechanism was applied to the detection of acute hepatopancreatic necrosis disease (AHPND) bacteria, reported by the same research group in 2016 [42].

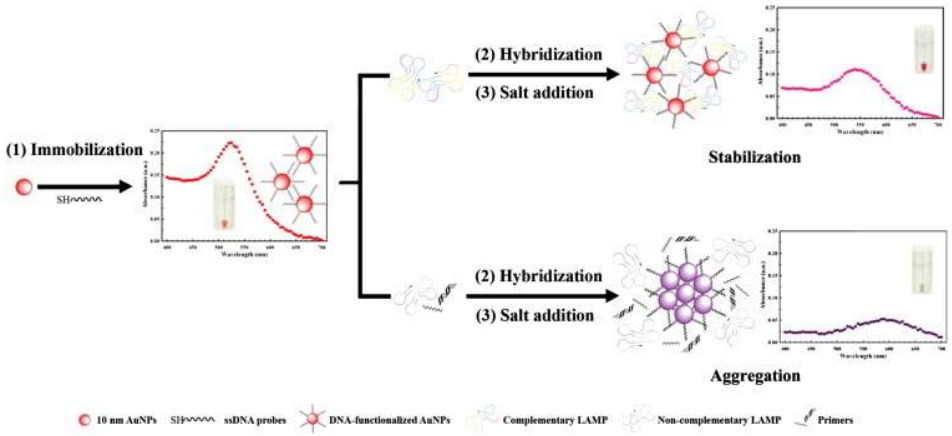

Figure 1.14. Schematic illustration of the detection of white spot syndrome virus (WSSV) using DNA-functionalized AuNPs as colorimetric probes (adapted from [41]).

Apart from oligo-AuNPs probes, unmodified AuNPs were also employed for the detection of isothermal amplification reactions. For instance, Ying, Jin, and co-workers reported that when a negative LAMP reaction product was mixed with unmodified AuNPs, the solution color remained red due to the rapid adsorption of dNTPs onto the AuNP surface, thereby stabilizing against salt-induced aggregation. In contrast, the amount of dNTPs in a positive LAMP reaction product was significantly reduced, and the mixing with unmodified AuNPs resulted in aggregation [43] (shown in Figure 1.15).

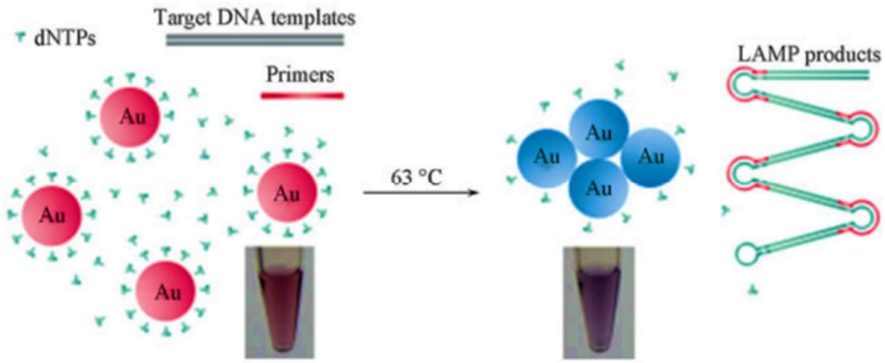

Figure 1.15. Schematic illustration of colorimetric detection of LAMP-based on the stabilization effect of dNTPs on AuNPs from aggregation (adapted from [43]).

1.3. Graphene-Based Materials for Nucleic Acid Detection

1.3.1. Graphene-Based Materials and Their Properties

In recent years, graphene-based materials have been widely used in versatile fields, such as electronics, optics, biology, and diagnostics. Graphene is a two-dimensional single-atom-thick carbon nanomaterial, and graphene oxide (GO), a highly oxidized version of graphene, has attracted considerable attention owing to its remarkable electronic, mechanical, and chemical properties [44]. Another graphene derivative, reduced graphene oxide (rGO) is commonly prepared by reducing GO, hence containing less oxygen functional groups (shown in Figure 1.16). Hydrophilic oxygen-containing functional groups on GO or rGO surfaces can help to stabilize dispersions in aqueous media. Moreover, these functional groups provide reactive handles for a variety of surface-modifications, which greatly increases their potential in various applications.

Commonly, GO is prepared based on the method reported by Hummers, where the oxidation of graphite to graphite oxide is accomplished by treating graphite with a water-free mixture of concentrated sulfuric acid (H_2SO_4), sodium nitrate ($NaNO_3$), and potassium permanganate ($KMnO_4$) [46]. This preparation method has the advantage of high cost-effectiveness due to the inexpensive graphite as raw material. Until now, a vast number of reduction methods has been reported to obtain rGO, such as chemical reagent reduction, thermal reduction, and microwave-assisted reduction. Among these methods, the chemical reduction is the most versatile one with many reduction agents being used, such as hydrazine [47–51], strong alkaline media [52], vitamin C or ascorbic acid [53], and sodium borohydride [54].

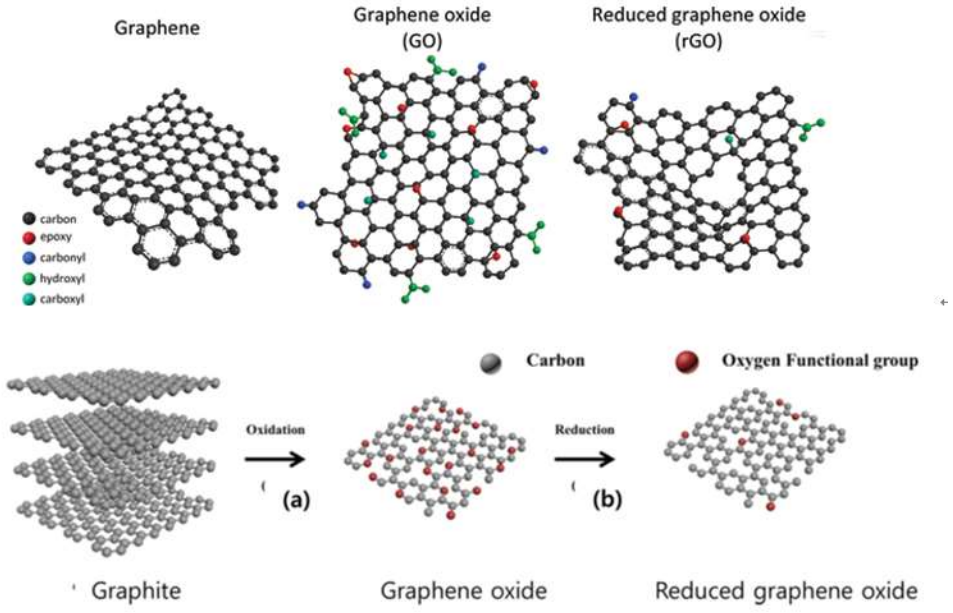

Figure 1.16. (Top) Schematic diagram of graphite, graphene oxide, and reduced graphene oxide. (Bottom) The process from graphite to GO and rGO (adapted from [45]).

It is well known that GO is water-soluble due to the hydrophilic oxygen-containing functional groups on their surface, such as hydroxyl, epoxide, and carboxylic groups. However, the aggregation of GO occurs in some specific chemical or physical conditions. The kinetics of GO aggregation have been studied by Gao and co-workers in 2013 [55]. Results showed that both pH and cation valence have significant effects on the aggregation of GO. As shown in Figure 1.17, when solution pH increases, protonation of carboxylic groups can decrease the stability of GO, resulting in a dominant mode of face-to-face aggregation. For cation valence, monovalent cation (Na^+) provides shielding to the charge surface to reduce the electric repulsive forces between GO sheets, thus improving the aggregation. However, ions with divalence (Mg^{2+} and Ca^{2+}) were found to be more effective than ions with monovalence (Na^+) in inducing the aggregation of GO. This can be explained that the divalent cations can additionally 'bridging' the functional groups at the edges of GO, which contributes to the cross-linking between GO sheets (edge-to-edge aggregation as dominant aggregation mode).

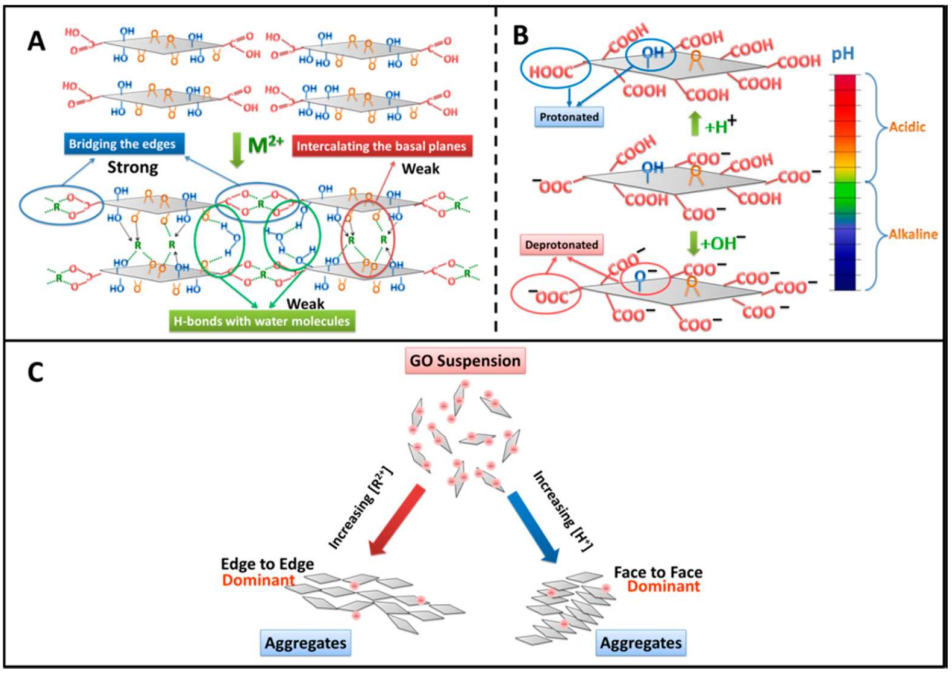

Figure 1.17. Schematic illustration of aggregation mechanisms of graphene oxide sheets (adapted from [56]).

1.3.2. Nucleic Acid Detection Using Graphene-Based Materials

Due to their extraordinary properties, graphene and its derivatives have been explored in a wide range of applications, such as electronic and photonic devices, clean energy, and sensors. Fluorescence resonance energy transfer (FRET) refers to a distance-dependent interaction between the excited states of two fluorescent dyes in which excitation is transferred from a donor to an acceptor without emission of a photon. As an effective quencher, GO has attracted considerable attention for FRET biosensors.

The strategies of these GO-based detection platforms are similar, relying on the effective quenching of fluorescence when dye-labeled probes are adsorbing on GO, and the presence of targets (e.g., thrombin or a designed complementary single-stranded DNA, ssDNA) induces

the desorption of probes through specific probe-target interactions, thereby the fluorescence recovers (shown in Figure 1.18).

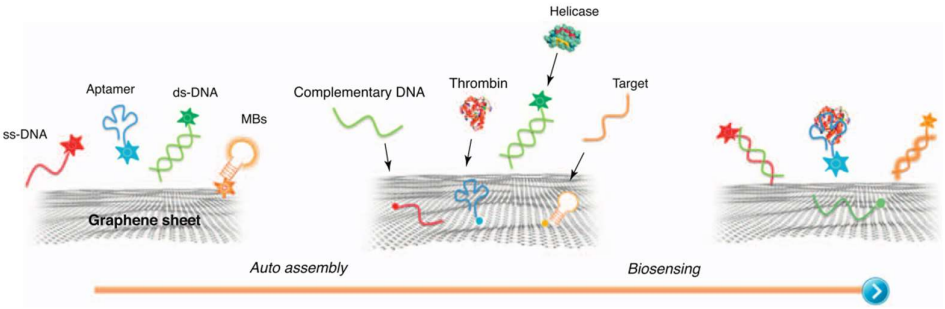

Figure 1.18. Schematic illustration of strategies of graphene and its derivate-based FRET detection platforms for various targets (adapted from [57]).

In 2009, Lu and co-workers pioneered the use GO for the detection of specific nucleic acid sequences [58]. Single-stranded DNA (ssDNA) sequences can adsorb on GO via π-stacking interaction and hydrogen bonding [59]. In this platform (scheme is shown in Figure 1.19), dye-labeled ssDNA could be quenched due to the binding with GO which is regarded as a strong quencher. The presence of target could release the dye-labeled ssDNA from GO, resulting in the restoration of the fluorescent signal. The platform was proved to be sensitive and have the advantage of low cost.

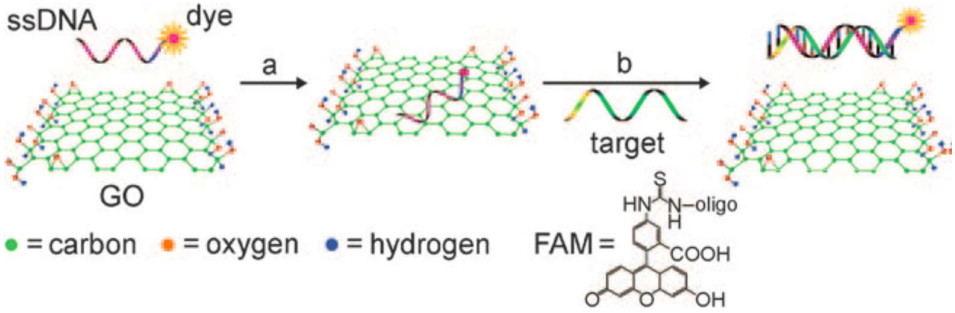

Figure 1.19. Schematic representation of the target-induced fluorescence recovers in GO-based nucleic acid detection platform (adapted from [58]).

In 2010, Fang, Fan, and co-workers demonstrated a platform for multicolor fluorescence DNA detection [60]. The scheme is shown in Figure 1.20. Due to the high quenching efficiency of GO, fluorescent dye-modified ssDNA probes exhibited minimal background fluorescence, while the fluorescence recovered after the hybridization of targets and complementary probes. It should be noted that the probes were modified using dyes with distinct colors to achieve the detection of multiple targets in the same solution. The limit of detection in this platform was determined to be as low as 100 pM.

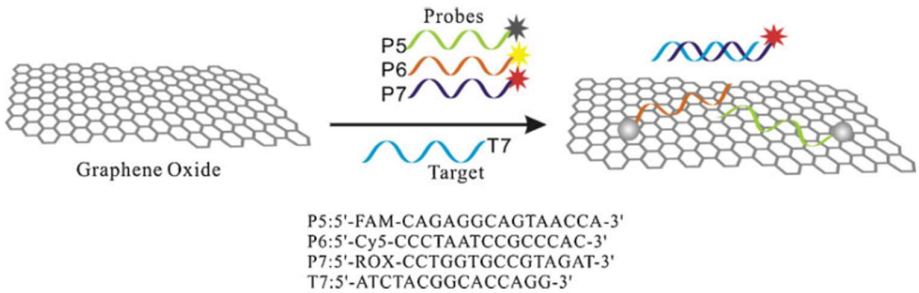

Figure 1.20. Schematic illustration of GO-based fluorometric detection for multiple DNA targets (adapted from [60]).

Another work utilizing graphene-based molecular beacon (MB) for nucleic acid detection was reported by Wang, Fan, and co-workers in 2010 [61]. In this work (Figure 1.21), the fluorescence of MB was firstly quenched by GO after the adsorption onto GO surface. The hybridization of complementary target and MB led to a dsDNA product, which showed the weaker affinity with GO. Therefore, the fluorescence signal recovered. And the MB without target remained quenched. Moreover, the single-mismatch differentiation ability of hairpin DNA was studied.

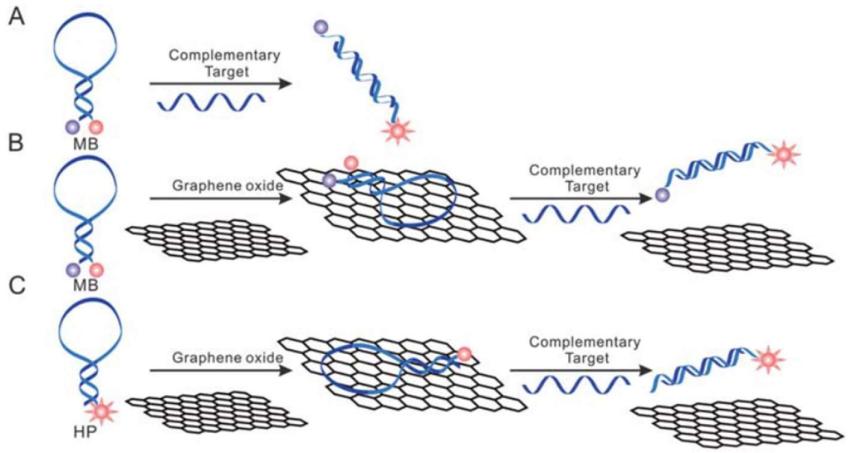

Figure 1.21. Schematic illustration of the graphene-based molecular beacon (MB) for nucleic acid detection (adapted from [61]).

Later in 2013, Wu and co-workers reported a fluorometric platform for dsDNA detection based on the significant quenching effect of GO [62]. The scheme is shown in Figure 1.22. The fluorescence of labeled single-stranded probes was quenched by GO in the absence of target. However, in the positive sample, dye-modified oligonucleotide probe could hybridize with the dsDNA target and formed a triplex DNA, which is more difficult to adsorb on the surface of GO than the probe. The limit

of detection was 14.3 nM.

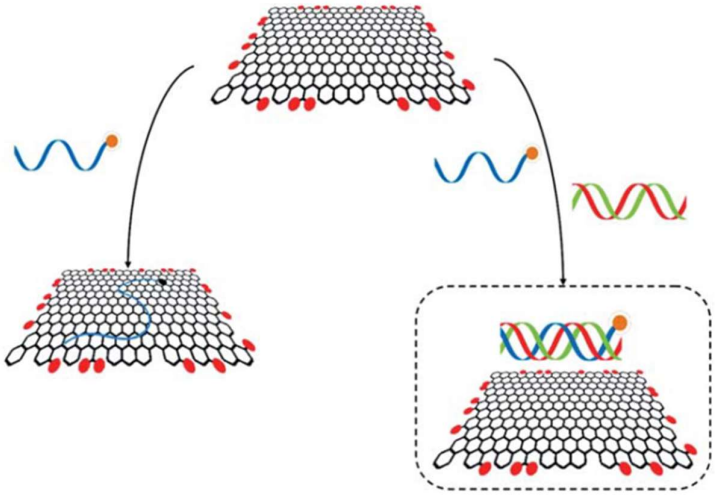

Figure 1.22. Schematic illustration of the GO-based platform for dsDNA detection (adapted from [62]).

In 2013, fluorescently labeled peptide nucleic acid (PNA) was demonstrated as probes for DNA detection by Zhang and co-workers [63]. PNA has been reported to possess more remarkable hybridization properties than oligonucleotides in terms of stability and sequence selectivity. As shown in Figure 1.23, the hybridization between target DNA and PNA probe induced a significant increase of fluorescence signal. The sensitivity of this platform was determined to be hundreds of picomolar.

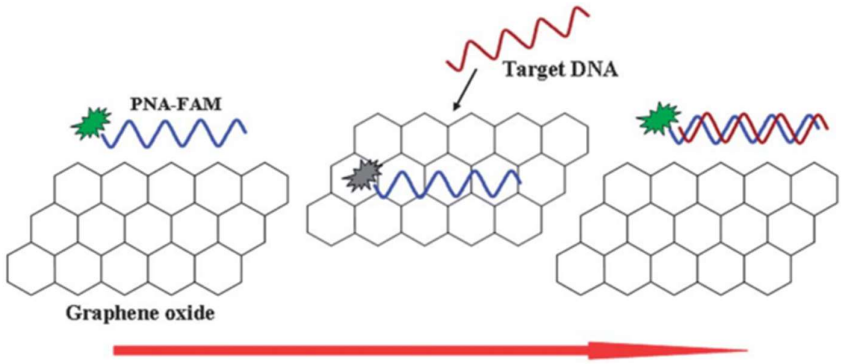

Figure 1.23. Schematic illustration of fluorescently labeled peptide nucleic acid (PNA) for GO-based DNA detection (adapted from [63]).

In many platforms, denaturation of dsDNA into single strands is necessary due to their detection mechanisms, which leads to the decrease of detection efficiency. To address this issue, another work using fluorescent dye-modified PNA as the probe was reported by Min and co-workers in 2014 [64]. In this work (shown in Figure 1.24), the superior binding affinity of PNA towards target dsDNA led to branch migration for gradual strand replacement, inducing the increase of fluorescence signal. The limit of this detection was 400 pM.

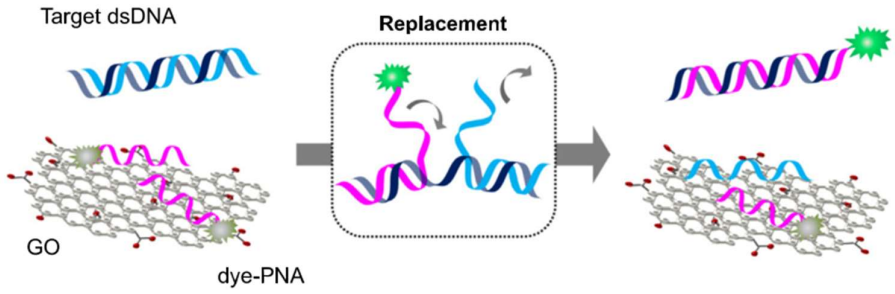

Figure 1.24. Schematic illustration of GO-based detection for dsDNA using peptide nucleic acid (PNA) as a probe (adapted from [64]).

It is reported that BSA can bind to GO via three possible interactions, i.e., π-stacking interaction, hydrophobic interaction, and hydrogen bonding [65]. In 2015, Min and co-workers further improved the previous PNA-based detection platform using BSA as an additive [66]. The scheme of this work is shown in Figure 1.25. BSA could inhibit the unfavorable adsorption of PNA/DNA duplex on GO surface, while still allowing the adsorption of PNA probes. Therefore, an improvement in the performance of this DNA detection platform was made, and the limit of detection was determined to be 0.5 nM, 90-folds lower than the previous PNA/GO-based DNA detection system.

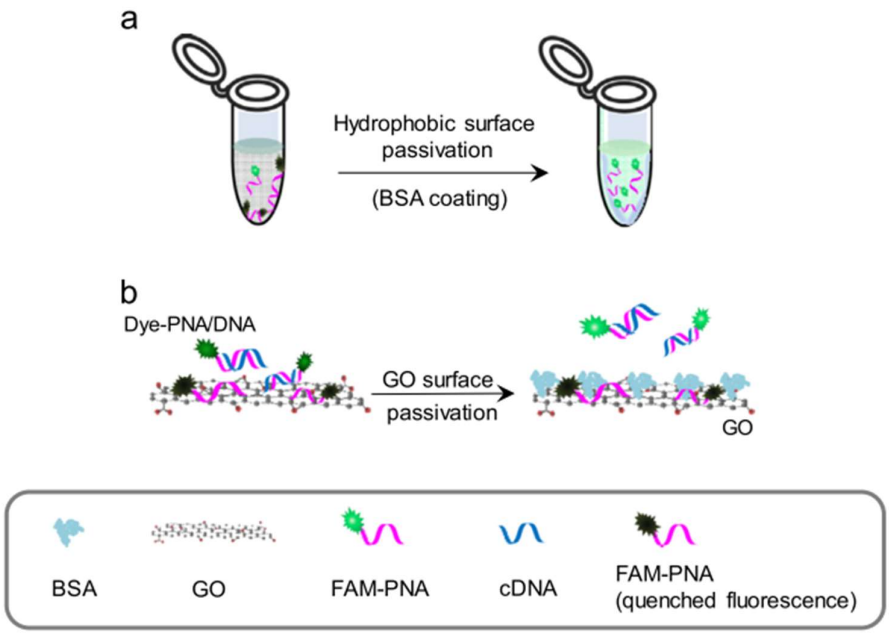

Figure 1.25. Schematic illustration of PNA/GO-based detection using bovine serum albumin as an additive to improve the sensitivity of detection (adapted from [66]).

More recently, in 2016, Chen and co-workers reported that the use of rGO could improve the detection sensitivity due to its higher quenching ability than GO [67]. Figure 1.26 shows the fluorescence intensity of

dye-modified ssDNA at various concentrations of GO and rGO. It is obvious that rGO showed a significantly higher quenching effect while GO only quenched around 35% at the same concentration, 5 μg mL^{-1}. Subsequently, rGO was used for the fluorometric detection of nucleic acid instead of GO. Results showed that the limit of detection could reach as low as 50 pM.

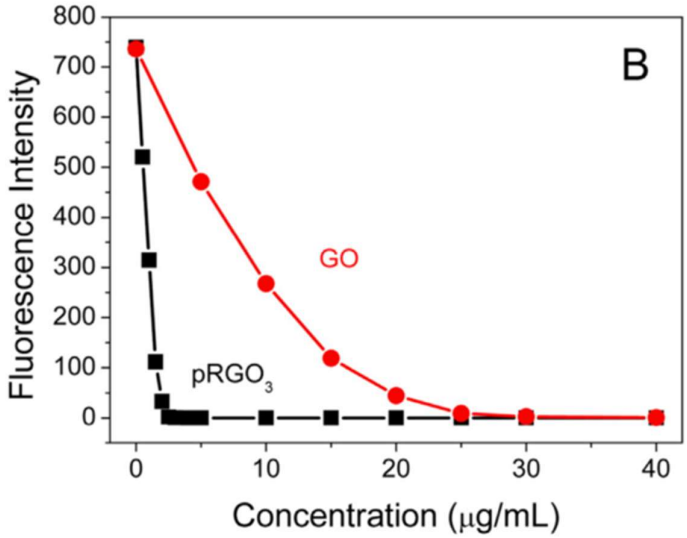

Figure 1.26. The dosage-dependent quenching effect of GO and $pRGO_3$ (reduced graphene oxide) (adapted from [67]).

Besides, there are also several GO-based fluorometric detection platforms combined with nucleic acid amplification reaction. In 2012, Zhang and co-workers reported a detection for multiple microRNA (miRNA) based on the fluorescence quenching of GO and strand displacement polymerase amplification (SDA) [68]. The scheme is shown in Figure 1.27. Multicolor fluorescent probes were used, and the recognition of specific target miRNA induced a strong emission after amplification, due to the low affinity of probe-miRNA duplex helix

towards GO. The limit of detection was 2.1 fM.

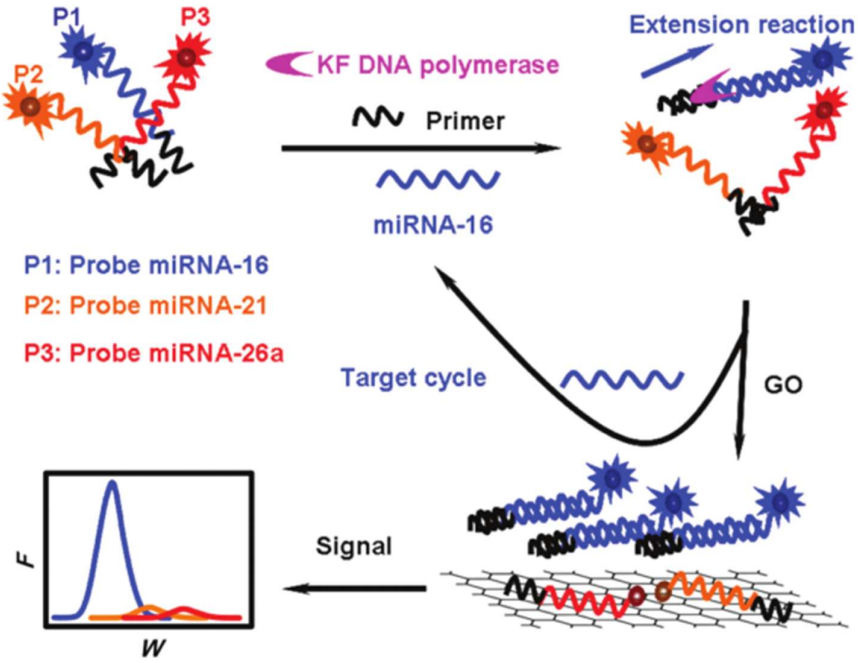

Figure 1.27. Illustration of the GO-based detection combined with strand displacement polymerase amplification for multiple miRNA (adapted from [68]).

In 2016, a fluorometric detection for miRNA based on the quenching effect of GO and rolling circle amplification (RCA) was demonstrated by Kim and co-workers [69]. In the scheme (Figure 1.28), target miRNA was firstly amplified by RCA, then the amplified product (long ssDNA) could be specifically hybridized with fluorescently labeled PNA probes, leading to the maintenance of fluorescence signal after the addition of GO. While the fluorescence signal in the sample without the target, miRNA was effectively quenched due to the adsorption of PNA probe onto GO surface.

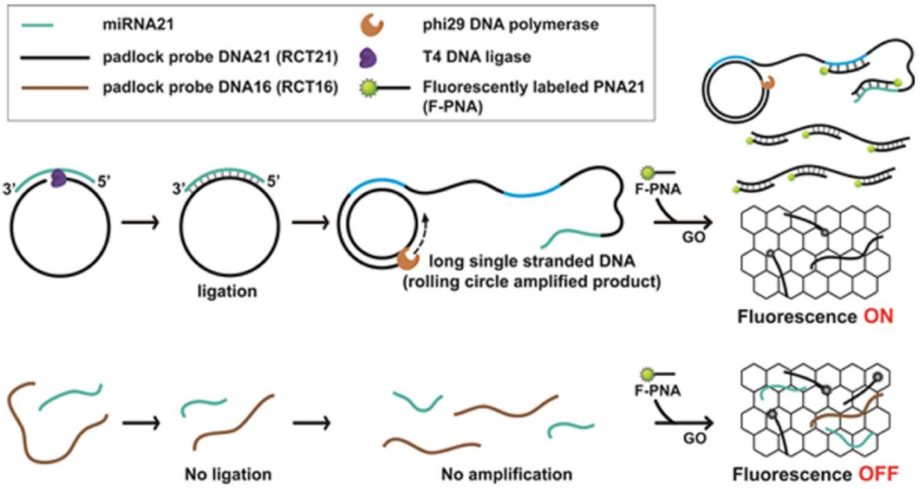

Figure 1.28. Schematic illustration of the GO-based platform combined with rolling circle amplification for miRNA detection (adapted from [69]).

Apart from fluorometric detection platforms based on the quenching effect of GO, there are several platforms using the aggregation of GO for DNA detection. In 2012, Li and co-workers demonstrated the self-assembly of GO was induced by DNA hybridization, which was then utilized for DNA detection [70]. The scheme is shown in Figure 1.29. Target DNA could hybridize with two ssDNA probes bound into different GO sheets, which caused the self-assembly of GO. Dynamic light scattering (DLS) measurement was used to detect the aggregation of GO which indicated the presence of target DNA. The limit of detection was determined to be 1 pM.

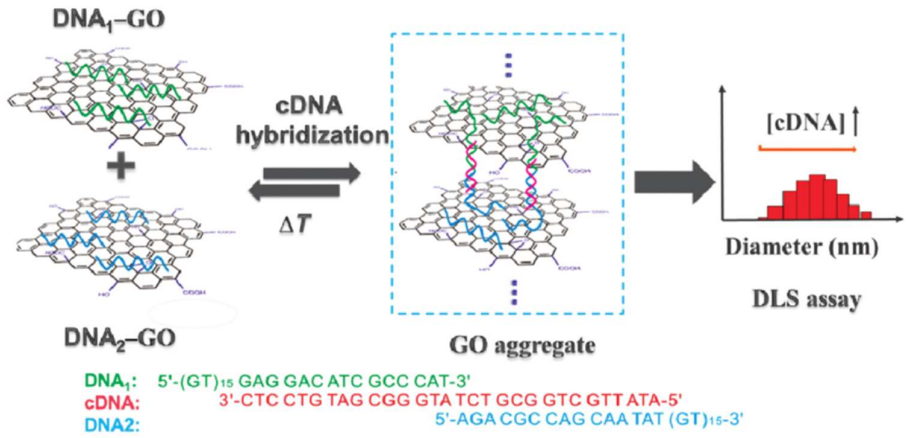

Figure 1.29. Schematic illustration of DNA-directed self-assembly of GO and the detection of DNA using dynamic light scattering (DLS) measurement (adapted from [70]).

More recently, in 2014, Li and co-workers reported a novel platform for the detection of specific DNA sequence based on the precipitation between GO and oligo-AuNPs [71]. The scheme of this platform is shown in Figure 1.30. ssDNA readily binds with GO via π-stacking interaction as well as hydrogen bonding. Therefore, when oligo-AuNPs were mixed with GO, cross-linking occurred. After 90 min, all the oligo-AuNPs were precipitated, and the supernatant became clear. The precipitation process can be monitored by measuring the absorbance of the residual oligo-AuNPs in the supernatant (surface plasmon resonance absorption peak at 525 nm). On the other hand, when the oligo-AuNPs were first hybridized with a complementary target sequence, no precipitation occurred upon the addition of GO. This is due to the base pairing of the double-stranded hybrid that prohibits the π-stacking interaction between DNA base and GO. The limit of detection of this platform by absorbance measurement was 7.5 nM whereas that by visual readout was not determined.

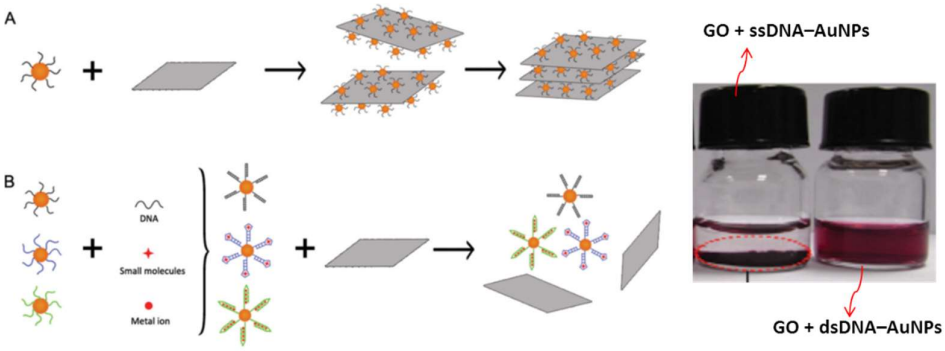

Figure 1.30. Schematic illustration of the precipitation-based platform conjugating GO and oligo-AuNPs for nucleic acid detection (adapted from [71]).

1.4. Challenges and Limitations of Existing Platforms for Nucleic Acid Detection

Nanomaterials have attracted considerable attention in recent years due to their ultrasmall size, large surface area-to-mass ratio, and high reactivity. Numerous efforts have been made to utilize nanomaterials in nucleic acid detection, such as AuNPs and graphene-based nanomaterials. Despite their intensive development, the existing nucleic acid detection platforms using AuNPs or graphene-based nanomaterials still have several research gaps yet to be addressed.

Nowadays, great emphasis is placed on point-of-care and on-site testing in resource-limited settings, which poses the need for platforms with the advantages of low cost, easy readout, and simple preparation. AuNPs have been extensively investigated in colorimetric platforms due to their unique optical properties. Oligo-AuNPs are prepared using thiol-modified oligonucleotides, which is expensive and time-consuming.

Another drawback of existing platforms is that the red and purple colors can sometimes be difficult to differentiate. These two limitations indicate the current AuNP-based detection platforms for nucleic acid are not suitable for point-of-care detection. Among graphene-based materials, GO are the most widely used material in fluorometric nucleic acid detection platforms because of their effective quenching ability of fluorescence dyes. The limitations of these fluorometric include the need for expensive labeling and fluorometer, which shows low potential to be used in resource-limited settings. Moreover, an immense potential has been shown to combine the detection with nucleic acid amplification to achieve the ultrasensitive detection platforms, whereas only a few of the related work has been reported due to the lack of effective detection strategies.

1.5. Objectives of This Study

a. To investigate the co-precipitation of bovine serum albumin-modified gold nanoparticles (BSA-AuNPs) with reduced graphene oxide (rGO).
b. To determine the optimal conditions for efficient co-precipitation of BSA-AuNPs with rGO.
c. To investigate the stabilization effect of single-stranded DNA (ssDNA) bound to rGO.
d. To demonstrate the precipitation-based detection of oligonucleotide target, polymerase chain reaction (PCR) product, and helicase-dependent amplification (HDA) product
e. To evaluate the performance of the platform in terms of sensitivity and specificity.

Chapter 2 Methodology

In this section, the methodology of the precipitation-based detection platform for nucleic acid amplification using bovine serum albumin-modified gold nanoparticles (BSA-AuNPs) and reduced graphene oxide (rGO) are presented. The detection scheme is introduced in Section 2.1, The materials and instruments used in experiments are listed in Section 2.2. The experiment protocol is given in Section 2.3.

2.1. Detection Scheme

It is demonstrated that bovine serum albumin (BSA) can serve as a 'universal glue' for subsequent assembly of gold nanoparticles on GO or rGO surface [65]. Inspired by the work of Li and co-workers that precipitation occurred when GO was mixed with single-stranded DNA (ssDNA)-modified AuNPs but not with double-stranded DNA (dsDNA)-modified AuNPs, we attempt to develop a novel precipitation-based detection platform for nucleic acid amplification using BSA-AuNPs and rGO. A schematic illustration of the precipitation-based platform with BSA-AuNPs and rGO is shown in Figure 2.1. In this scheme, rGO is firstly incubated with the amplification reaction product for 1 h. For negative sample (without the target), the unused single-stranded primers can stabilize the rGO from salt-induced aggregation. Hence, no precipitates will form, and reaction mixture remains dispersed in red after adding BSA-AuNPs and 1 h incubation at 65 °C. For positive sample (with the target), the incubation with double-stranded amplification product is not able to stabilize the rGO from the salt-induced aggregation. Thus, precipitation appears after the addition of

BSA-AuNPs and the subsequent 1 h incubation at 65 °C. First, the co-precipitation effects of BSA-AuNPs with rGO will be studied for the determination of optimal conditions. Subsequently, the precipitation-based platform will be utilized for oligonucleotide target detection. The applicability for nucleic acid amplification detection will then be investigated with polymerase chain reaction (PCR) and helicase-dependent amplification (HDA) products. Last, specificity and sensitivity tests for the detection of each amplification reaction will be conducted to evaluate this new platform.

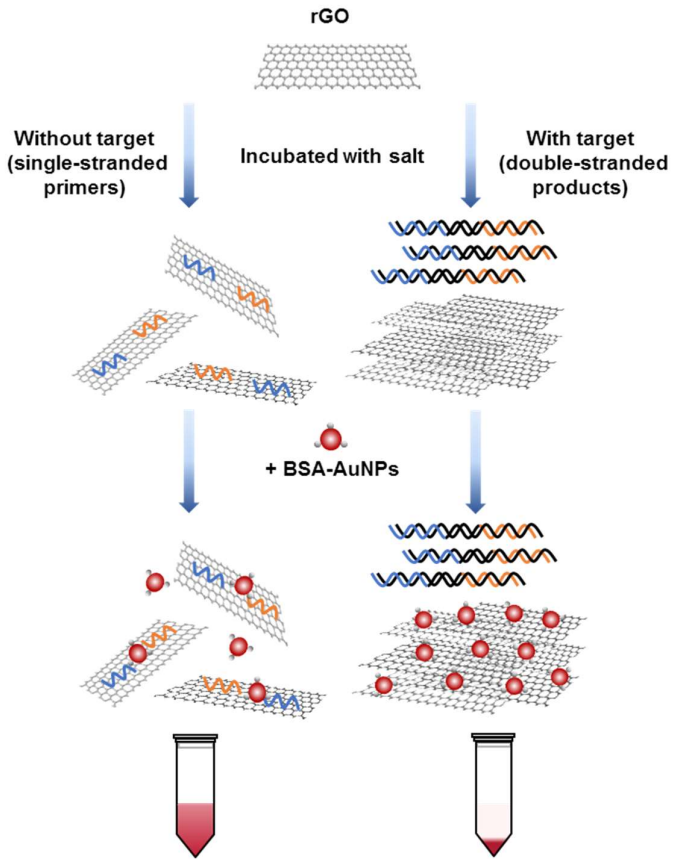

Figure 2.1. Schematic illustration of the precipitation-based detection of DNA amplification reaction using the BSA-AuNPs and rGO. (Left tube) without target: dispersed red; (right tube) with target: precipitated red.

2.2. Materials and Instruments

Hydrochloric acid, nitric acid, sodium hydroxide, hydrogen tetrachloroaurate (III), bovine serum albumin (BSA), sodium borohydride, Tween 20, sodium chloride, ammonium sulfate ($(NH_4)_2SO_4$), ultrapure agarose, and tris(hydroxymethyl)aminomethane (Tris) were purchased from Sigma-Aldrich. Nano graphene oxide (GO) solution was purchased from Graphene Supermarket. UltraPure DNase/RNase-free distilled water (UltraPure water), and gel loading buffer (BlueJuice) was purchased from Invitrogen. All DNA oligonucleotides were synthesized and purified by Integrated DNA Technologies. Reagents for PCR (i.e., Taq polymerase, Deoxynucleotide (dNTP) solution, standard 10X Taq reaction buffer), IsoAmp II Universal tHDA Kit for helicase-dependent amplification (HDA) reaction, ΦX174 RF I DNA, lambda DNA, and low molecular weight DNA ladder were from New England Biolabs. Distilled water was from Direct-Q 3 system (Millipore; 18.2 MΩ·cm; fitted with a Millipak Express 20 filter). All solutions were prepared with UltraPure water.

Centrifugation was performed by a Centrifuge 5415D (Eppendorf). Sonication was conducted using a WiseClean WUC-A01H ultrasonic cleaner (Daihan Scientific). Shaking was by a Thermomixer compact (Eppendorf). Transmission electron microscopy (TEM) was performed using a JEM-2100F field emission electron microscope (JEOL). Fourier transform infrared spectroscopy (FTIR) was performed by Bruker Vertex 70 FTIR spectrometer (Rheinstetten). Ultraviolet/visible spectrum was measured using an Ultrospec 2100 pro UV/visible spectrophotometer (GE Healthcare). Dynamic light scattering (DLS) and zeta potential

measurements were conducted by a Zetasizer Nano ZS (Malvern; 633 nm He–Ne laser). Gel electrophoresis was visualized by a Gel Doc XR+ System (Bio-Rad). Isothermal incubation and thermal cycling were carried out using GeneAmp PCR system 9700 (Applied Biosystems).

2.3. Experiment Protocol

2.3.1. Preparation and Characterization of BSA-AuNPs and rGO

Gold nanoparticles were synthesized based on the reported citrate reduction method [16]. All glassware and magnetic stir bar used in the AuNPs synthesis were cleaned with aqua regia (the mixture of concentrated hydrochloric acid and nitric acid in a volume ratio of 3:1), rinsed with distilled water, and dried in an oven. A solution of hydrogen tetrachloroaurate (III) (30 mL, 0.01 wt%) was boiled under reflux with vigorous stirring. After rapid addition of 3 mL sodium citrate (1 wt%), the solution color changed from pale yellow to wine red within minutes. Heating and stirring were continued for 15 min, followed by cooling to room temperature under stirring. Prior to the conjugation with BSA, the AuNPs solution was concentrated by centrifugation (5,800 rpm for 45 min). BSA solution (25 mg mL^{-1}) was prepared and added rapidly into concentrated AuNPs solution. AuNPs (20 nM) and BSA (1 mg mL^{-1}) were incubated for 24 h under shaking at 1000 rpm. The as-synthesized AuNPs and BSA-AuNPs solutions were stored at 4 °C until use. The as-synthesized AuNPs and BSA-AuNPs were characterized by visible spectrophotometry and DLS.

To prepare rGO, GO solution (1g L^{-1}, 2.5 mL) was first sonicated for 20 min, followed by mild stirring at room temperature. Freshly prepared

$NaBH_4$ solution (200 mM, 2.5 mL) was then added into the above GO solution under vigorous stirring in a dropwise manner. After overnight incubation under stirring, the resultant black solution was centrifuged (9000 rpm for 15 min) and washed with UltraPure water for 3 times. The purified products were redispersed in UltraPure water by sonication for 10 min and stored at room temperature until use. GO and as-prepared rGO were characterized by visible spectrophotometry, FTIR as well as DLS and zeta potential measurements.

2.3.2. Salt-Induced Aggregation Behavior of rGO

rGO (10 μg mL^{-1}) was firstly incubated with different concentrations of NaCl (0–0.1 M) at room temperature for 3 h, followed by centrifugation at 2000 rpm for 1 min to precipitate the aggregated rGO. The supernatant was collected, and the absorbance at 244 nm was measured. For GO, similar experiments were carried out for comparison and absorbance at 230 nm was measured.

2.3.3. Stability of BSA-AuNPs

BSA-AuNPs (2 nM) were adjusted to different pHs (4, 5, 6, 7, 8, and 9), followed by 1 h incubation at 65 °C. Zeta potential measurement of BSA-AuNPs in different pHs (4, 5, 6, 7, 8, and 9) was conducted. Similar experiments were carried out with AuNPs for comparison. pHs were adjusted by adding 1 M HCl or NaOH.

2.3.4. Co-precipitation of BSA-AuNPs with rGO

rGO (8.75 μg mL^{-1}) was first incubated in aggregation buffer (20 mM Tris-HCl, 50 mM NaCl, 10 mM $(NH_4)_2SO_4$, 0.05% Tween 20; pH 7.4) at room temperature for 1 h, followed by the addition of BSA-AuNPs (2 nM).

The mixture of BSA-AuNPs and rGO was then incubated at 65 °C for 1 h. After that, the absorbance of the supernatant was measured at 528 nm. TEM was used to characterize the red precipitates.

For effects of components of reaction buffer on the co-precipitation of BSA-AuNPs with rGO, rGO (8.75 μg mL^{-1}) was first incubated in different components at room temperature for 1 h, followed by the addition of BSA-AuNPs (2 nM). The mixture of BSA-AuNPs and rGO was then incubated at 65 °C for 1 h. For effect of pH, rGO (8.75 μg mL^{-1}) was first incubated with 50 mM NaCl at room temperature for 3 h. After the addition of BSA-AuNPs (2 nM), the mixture of BSA-AuNPs and rGO was adjusted to different pHs (4, 5, 6, 7, 8, and 9), followed by the incubation at 65 °C for 1 h. For effect of rGO concentration, different concentrations of rGO (0, 2.75, 4.75, 6.75, 8.75, and 10.75 μg mL^{-1}) were incubated in aggregation buffer at room temperature for 1 h. After the addition of BSA-AuNPs (2 nM), the mixture was incubated at 65 °C for 1 h. For effect of incubation time of rGO in aggregation buffer, rGO (8.75 μg mL^{-1}) was incubated in aggregation buffer at room temperature for different time (0, 30, 60, 90, and 120 min). After the addition of BSA-AuNPs (2 nM), the mixture was incubated at 65 °C for 1 h. For effect of incubation temperature after adding BSA-AuNPs, rGO (8.75 μg mL^{-1}) was first incubated in aggregation buffer at room temperature for 1 h. After the addition of BSA-AuNPs (2 nM), the mixture was incubated at different temperatures (25, 45, 65, and 85 °C) for 1 h. For effect of BSA concentration in the preparation BSA-AuNPs, different BSA concentrations (0, 1, and, 5 mg mL^{-1}) were used with the concentration of AuNPs kept at 20 nM during the preparation of BSA-AuNPs. Then, the three kinds of as-prepared BSA-AuNPs (2 nM) were added to rGO

after the 1 h incubation of rGO (8.75 μg mL^{-1}) in aggregation buffer at room temperature. Then the mixture of BSA-AuNPs and rGO was incubated at 65 °C for 1 h. The absorbance values were all measured at 528 nm.

2.3.5. Stabilization Effect of ssDNA on rGO

rGO (8.75 μg mL^{-1}) was first incubated with different concentrations of ssDNA (0–150 nM; 5'-TACAGTCATAGATGGTCGGTGGGAGGTGG-3') in aggregation buffer (20 mM Tris-HCl, 50 mM NaCl, 10 mM $(NH_4)_2SO_4$, 0.05% Tween 20; pH 7.4) at room temperature for 1 h, followed by the addition of BSA-AuNPs (2 nM). Then, the mixture was incubated at 65 °C for 1 h. The absorbance values were all measured at 528 nm. Similar experiments were carried out with dsDNA for comparison by using ssDNA (0–150 nM) and same concentrations of its complementary sequence (0–150 nM; 5'-CCACCTCCCACCGACCATCTATGACTGTA-3') for the incubation with rGO.

For DLS analysis, rGO was incubated with 100 nM ssDNA or dsDNA in aggregation buffer at room temperature for 1 h before measurements. rGO without DNA was included for comparison.

2.3.6. Precipitation-Based Detection of Oligonucleotide Target Using BSA-AuNPs and rGO

rGO (8.75 μg mL^{-1}) was first incubated with probe sequence (100 nM; 5’-TACAGTCATAGATGGTCGGTGGGAGGTGG-3’) as well as target DNA sequence (0–100 nM; 5’-CCACCTCCCACCGACCATCTATGACTGTA-3’) in aggregation buffer

(20 mM Tris-HCl, 50 mM NaCl, 10 mM $(NH_4)_2SO_4$, 0.05% Tween 20; pH 7.4) at room temperature for 1 h, followed by the addition of BSA-AuNPs (2 nM). The mixture of BSA-AuNPs and rGO was then incubated at 65 °C for 1 h. After that, the absorbance of the supernatant was measured at 528 nm.

2.3.7. Precipitation-Based Detection of PCR and HDA Products Using BSA-AuNPs and rGO

For PCR product detection, PCR samples were prepared with 1X standard Taq reaction buffer (10 mM Tris-HCl, 50 mM KCl, 1.5 mM $MgCl_2$; pH 8.3), dNTPs (0.1 mM each), Primer 1 (5'-CTGCTCCTGTTGAGTTTATTGC-3', 0.6 mM), Primer 2 (5'-GCGAACAATTCAGCGGCTTTA-3', 0.6 mM), Taq DNA polymerase (0.025 units mL^{-1}), and the target (ΦX174 DNA for a positive sample, 10^7 copies; UltraPure water for a negative sample). The profile used for thermal cycling was 94 °C for 2 min (initial denaturation); 35 cycles of 94 °C for 15 s (denaturation), 55 °C for 15 s (annealing), and 72 °C for 30 s (extension); and 72 °C for 2 min (final extension). After cooling to room temperature, the PCR samples (3-fold dilution) were added to rGO. Subsequent experiments were identical to those for the 29-base oligonucleotide target. For HDA product detection, HDA samples were prepared with 1X annealing buffer (20 mM Tris-HCl, 10 mM KCl; pH 8.8), $MgSO_4$ (4 mM), NaCl (40 mM), 0.07X IsoAmp® dNTP solution, forward primer (5'-AGCCGAATTCAAAACATCGTAACTGAG-3', 0.2 mM), reverse primer (5'-AATATTTTCCAACAACGCTTCTGCAAT-3', 0.2 mM), 0.07X IsoAmp® enzyme mix, and the target (pCNG1 DNA for a positive sample, 500000 copies; UltraPure water for a negative sample). The incubation was carried at 65 °C for 90 minutes using a thermocycler.

After cooling to room temperature, the HDA samples (4-fold dilution) were added to rGO. Subsequent experiments were identical to those for the 29-base oligonucleotide target. For specificity test, lambda DNA was utilized as the non-specific target for both PCR and HDA detection. For sensitivity test, different copies of ΦX174 DNA (0, 0, 10^3, 10^4, 10^5, 10^6, and 10^7 copies) were used for PCR product detection, while different copies of pCNG1 DNA (0,50, 500, 5000, 50000, and 500000 copies) were used for HDA product detection. For gel electrophoresis, PCR or HDA products (9 μL, plus 1 μL BlueJuice gel loading buffer) were loaded into wells of an agarose gel (2%) in 0.5X TBE buffer (45 mM Tris, 45 mM boric acid, 1 mM EDTA; pH 8.0) and subjected to electrophoresis at 120 V for 50 min. The gel was then stained with 1X SYBR gold for 30 min and visualized by UV transillumination.

Chapter 3 Results and Discussion

3.1. Synthesis and Characterization of BSA-AuNPs and rGO

Gold nanoparticles (AuNPs) were synthesized based on the citrate reduction method, and bovine serum albumin-modified gold nanoparticles (BSA-AuNPs) were prepared by mixing AuNPs and BSA solution. As shown in Figure 3.1, there was a slight change of the solution color from coral red to cerise after the modification of gold nanoparticles with BSA molecules.

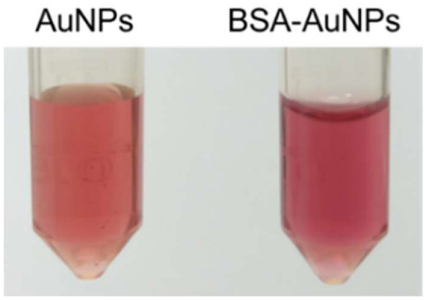

Figure 3.1. Photograph showing the appearance of gold nanoparticles (AuNPs) and bovine serum albumin-modified AuNPs (BSA-AuNPs). The concentration of the two solutions was 4.46 nM.

The visible absorption spectra of AuNPs and BSA-AuNPs were obtained (Figure 3.2 (top)). AuNPs have the peak absorbance at 520 nm while that of BSA-AuNPs redshifted to 528 nm, indicating a slight red-shift caused by the adsorption of BSA on the surface of AuNPs. The size and concentration of the AuNPs were estimated from the absorbance data according to the method reported by Haiss and co-workers [72]. Based on the ratio of the absorbance at the SPR peak to the absorbance at 450 nm, the size of the AuNPs was determined to be ~15 nm. The

concentration of the AuNPs solution was calculated to be 4.46 nM. Besides, the dynamic light scattering (DLS) results (Figure 3.2 (bottom)) indicated the mean values of the hydrodynamic sizes of AuNPs and BSA-AuNPs were 21.5 nm and 34.9 nm, respectively, further suggesting the successful preparation of BSA-AuNPs.

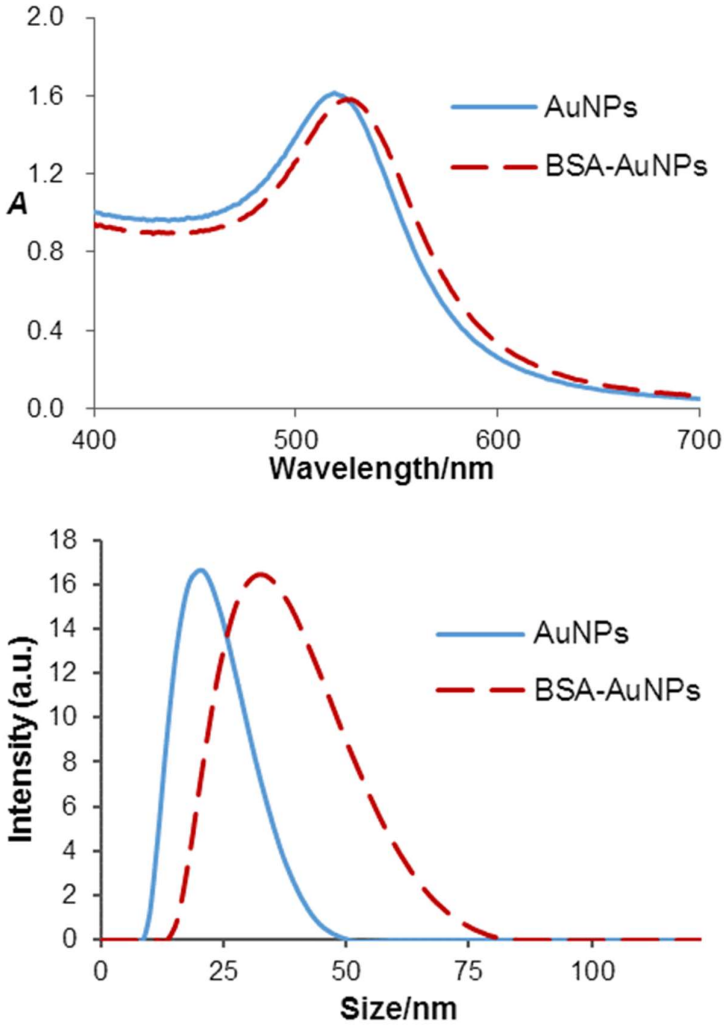

Figure 3.2. (Top) Visible absorption spectra of AuNPs and BSA-AuNPs. (Bottom) Dynamic light scattering (DLS) results of AuNPs and BSA-AuNPs.

For the characterization of graphene oxide (GO) and reduced graphene oxide (rGO), the appearance of their solutions is presented in Figure 3.3. It is obvious that rGO shows darker brown in color than GO at the same concentration. It is noteworthy that the rGO formed black precipitates due to the partial removal of negatively charged functional groups after the reduction using $NaBH_4$. However, the rGO precipitates could be redispersed in water by means of sonication.

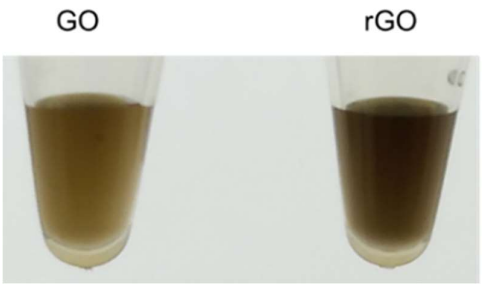

Figure 3.3. Photograph showing the appearance of graphene oxide (GO) and reduced graphene oxide (rGO). The concentration of the two dispersions was 500 μg mL^{-1}.

The absorption spectra of GO and rGO were measured with UV/Visible spectrophotometer (Figure 3.4 (a)). GO shows an absorption peak at 230 nm, which shifts to 244 nm upon the reduction by $NaBH_4$. This red shift further demonstrates the successful reduction to rGO which possesses less functional groups on the surface. Figure 3.4 (b) presents the DLS results of GO and rGO, indicating the average hydrodynamic sizes of GO and rGO were 232.8 nm and 238.7 nm, respectively. These results illustrated that the reduction of GO did not cause significant size change. In addition, Figure 3.4 (c) suggests that the zeta potential values of GO and rGO were −41.3 mV and −38.4 mV, respectively, which is attributed to the decrease of functional groups after reduction.

Moreover, Fourier transform infrared (FTIR) spectra of GO and rGO are presented in Figure 3.4 (d). Obviously, the spectrum of GO showed that absorption peaks at 1730, 1623, and 1043 cm^{-1}, which are attributed to C=O, C=C, and C–O groups, respectively. Nevertheless, for rGO, the absorption peak at around 1730 cm^{-1} disappeared, which indicated the absence of C=O group after reduction. The peak at 1590 cm^{-1}, related to C=C group, and the peak at 1083 cm^{-1} which is due to C–O group, were still existed. These results demonstrated the successful preparation of rGO using $NaBH_4$, as partial functional groups of GO were effectively eliminated.

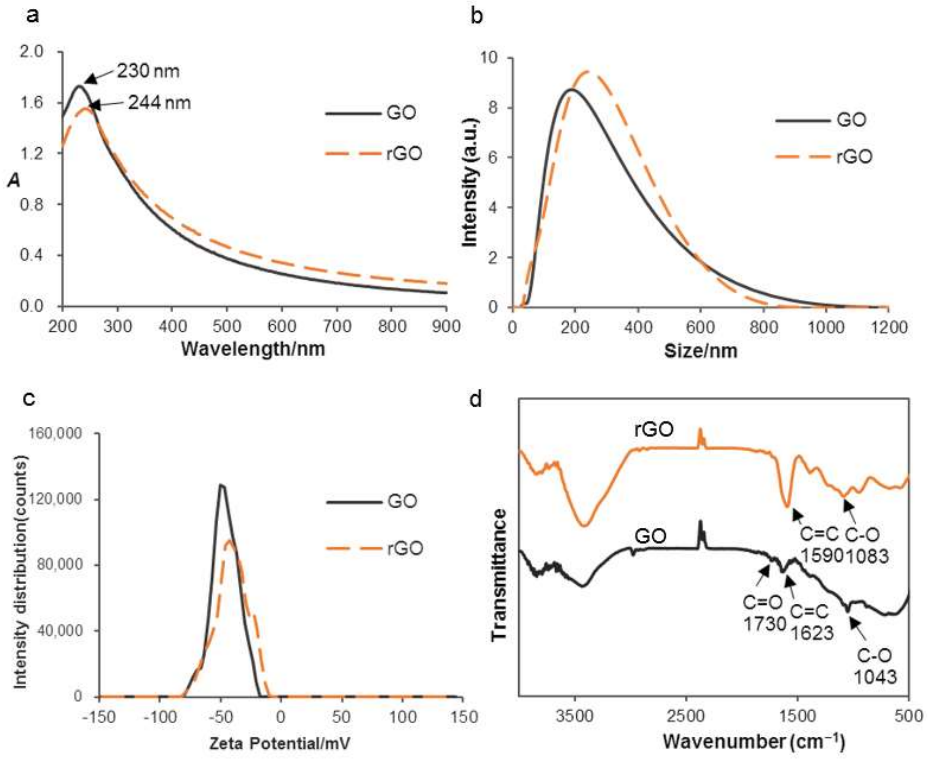

Figure 3.4. Characterization of GO and rGO. (a) Ultraviolet-visible absorption spectra of GO and rGO. (b) DLS results of GO and rGO. (c) Zeta potential results of GO and rGO. (d) Fourier transform infrared (FTIR) spectra of GO and rGO.

Transmission electron microscopy (TEM) photographs of AuNPs, BSA-AuNPs, GO, and rGO were obtained. As shown in Figure 3.5, both AuNPs and BSA-AuNPs had uniform sizes of around 15 nm in diameter, which is consistent with the estimated sizes from UV/Visible spectrometry. It is noteworthy that the interparticle distance between BSA-AuNPs was larger than that between AuNPs due to the modification of BSA which contributes to hydrodynamic sizes of BSA-AuNPs and possibly increases the electrostatic repulsion between nanoparticles. TEM images of GO and rGO both showed single or a few layers of structures with wrinkles and defects on the surfaces. The sizes of GO and rGO sheets were approximately 238.7 and 232.8 nm, respectively.

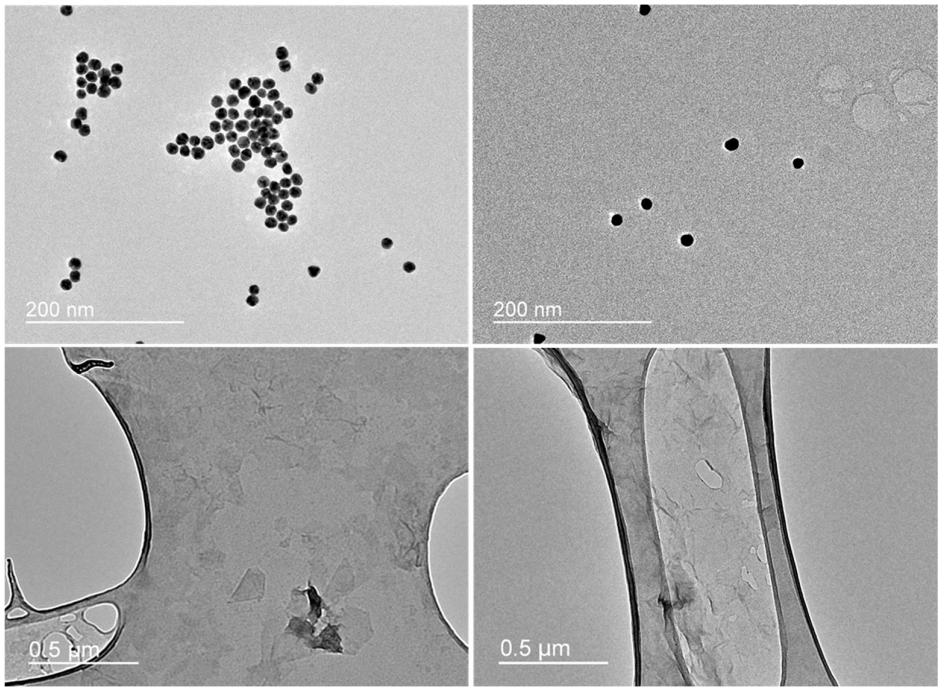

Figure 3.5. Transmission electron microscopy (TEM) photographs of (top left) AuNPs, (top right) BSA-AuNPs, (bottom left) GO, and (bottom right) rGO.

3.2. Salt-Induced Aggregation Behavior of rGO

Salt-induced aggregation behavior of rGO was studied using UV/Visible spectrometry. In the study, rGO was firstly incubated with different concentrations of NaCl for 3 h, followed by centrifugation to precipitate the aggregated rGO. The amount of aggregated rGO was detected by the decrease in absorbance of the supernatant at 244 nm. GO was included for comparison with absorbance measured at 230 nm. As shown in Figure 3.6, most of the rGO was dispersed with 0–20 mM NaCl while aggregated efficiently with 50 mM NaCl or higher concentrations. At 40 mM NaCl, only half of the GO was aggregated while severe aggregation occurred for rGO. Compared with GO, rGO showed lower stability against salt-induced aggregation, which can be explained by the less surface charge after reduction by $NaBH_4$ due to the removal of partial oxygen functional groups. It is obvious that rGO shows higher potential to form aggregates than GO, and 50 mM NaCl is nearly as effective as 100 mM NaCl in terms of inducing the aggregation of rGO.

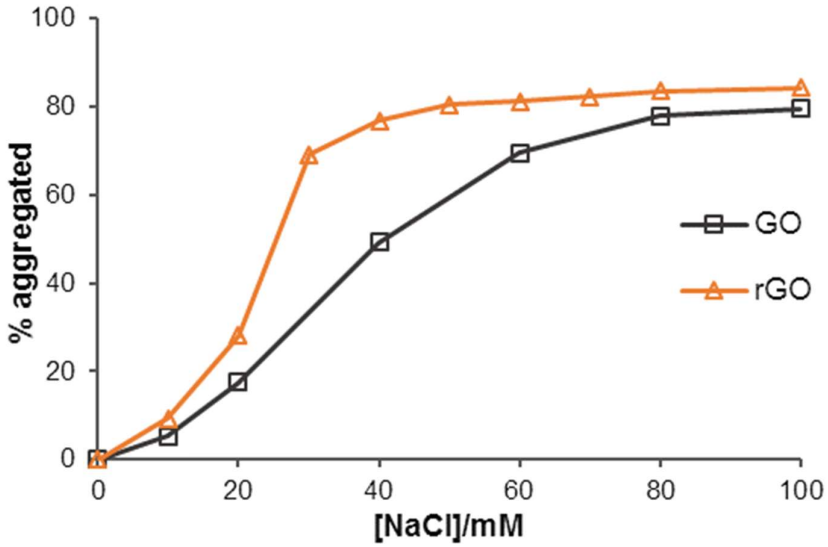

Figure 3.6. Salt-induced aggregation behavior of rGO compared with GO. The concentration of rGO and GO was 10 μg mL^{-1}. The two kinds of nanomaterials were firstly incubated with different concentrations of NaCl for 3 h, followed by centrifugation to precipitate the aggregated rGO or GO. Percentages aggregated of rGO and GO were detected by the decrease in absorbance of the supernatant at 244 nm and 230 nm, respectively.

3.3. Stability of BSA-AuNPs

To study the stability of BSA-AuNPs, BSA-AuNPs at different pHs were incubated at 65 °C for 1 h, and zeta potential values of BSA-AuNPs at different pHs were measured. The results are presented in Figure 3.7. After 1 h incubation at 65 °C, BSA-AuNPs at pH 5 was precipitated while remained dispersed at other pH values (4, 6, 7, 8, and 9). The zeta potential results of BSA-AuNPs at various pHs (Figure 3.7 (bottom)) indicates that BSA-AuNPs showed an isoelectric point (IEP) at 4.6, which is consistent with BSA. At pH lower than 4.6, the surface of BSA-

AuNPs was positively charged and changed to negatively charged if pH is higher than 4.6. It is obvious that among these six pH values, the electrostatic repulsion was the lowest at pH 5 as the zeta potential was highly close to zero, which can explain the precipitation of BSA-AuNPs at pH 5.

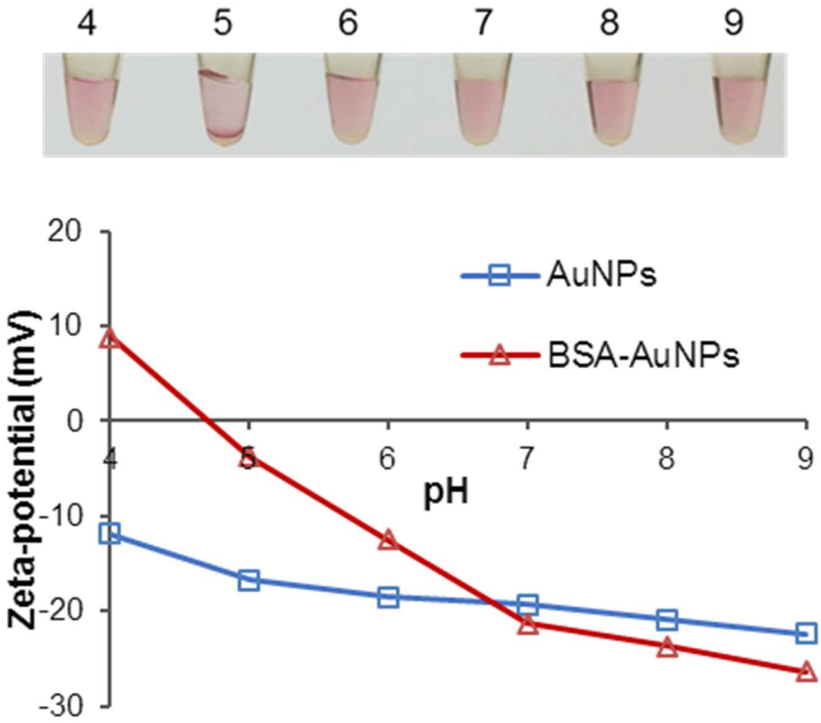

Figure 3.7. (Top) Photograph showing BSA-AuNPs in different pHs (4, 5, 6, 7, 8, and 9) after 1 h incubation at 65 °C. The concentration of BSA-AuNPs was 2 nM. (Bottom) Plots of zeta potential of AuNPs and BSA-AuNPs in different pHs (4, 5, 6, 7, 8, and 9). pHs were adjusted by 1 M NaOH or HCl.

3.4. Co-precipitation of BSA-AuNPs with rGO

To demonstrate the co-precipitation of BSA-AuNPs with rGO, different

nanomaterials were incubated in aggregation buffer (20 mM Tris-HCl, 50 mM NaCl, 10 mM $(NH_4)_2SO_4$, 0.05% Tween 20; pH 7.4), and Figure 3.8 presents their appearances after 1 h incubation at 65 °C. In the third tube (from left to right), the mixture containing BSA-AuNPs and rGO remained dispersed. Interestingly, for the last tube, rGO was incubated in aggregation buffer for 1 h at room temperature, then BSA-AuNPs were added to rGO. After 1 h incubation at 65 °C, red precipitates occurred, and the supernatant became almost colorless. This result was believed due to the 1 h incubation of rGO in aggregation buffer before the addition of BSA-AuNPs led to the effective salt-induced aggregation of rGO, while rapid mixing of BSA-AuNPs and rGO in buffer could not result in the happening of red precipitates due to instant adsorption of BSA-AuNPs on rGO, protecting rGO from salt-induced aggregation. These results suggested that the co-precipitation of BSA-AuNPs with rGO only occurred when BSA-AuNPs were mixed with aggregated rGO instead of dispersed rGO. The TEM image of the red precipitates is shown in Figure 3.8 (bottom), which showed that a great number of BSA-AuNPs were adsorbed on rGO. Besides, rGO alone in aggregation buffer should be aggregated but still showed colorless, and BSA-AuNPs alone remained dispersed after 1 h incubation at 65 °C, indicating the higher stability in pH 7.4 aggregation buffer compared with pH 5.

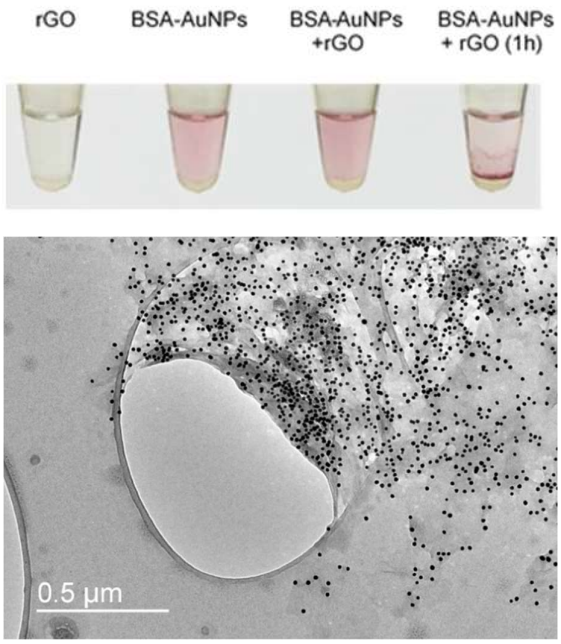

Figure 3.8. (Top) Photograph showing different nanomaterials in aggregation buffer (20 mM Tris-HCl, 50 mM NaCl, 10 mM $(NH_4)_2SO_4$, 0.05% Tween 20; pH 7.4) after 1 h incubation at 65 °C: (from left to right) rGO, BSA-AuNPs, BSA-AuNPs plus rGO, and BSA-AuNPs plus rGO which were incubated for 1 h at room temperature before the addition of BSA-AuNPs. The concentrations of BSA-AuNPs and rGO in all samples (if possible) were 2 nM and 8.75 µg mL^{-1}, respectively. (Bottom) TEM image of red precipitates shown in the last tube (from left to right).

Based on the precipitation test demonstrating that BSA-AuNPs only precipitated with aggregated rGO but remained dispersed with dispersed rGO, we proposed a scheme illustrating the co-precipitation of BSA-AuNPs with rGO. As shown in Figure 3.9, rGO remained dispersed without pre-incubation with aggregation buffer. After the addition of BSA-AuNPs, BSA-AuNPs adsorb onto rGO instantly which can stabilize rGO from further aggregation, therefore there is no observable precipitation after 1 h incubation. However, the incubation

with aggregation buffer can result in the aggregation of rGO, thus significantly larger sizes of rGO aggregates formed with considerable binding sites for BSA-AuNPs. Subsequently, BSA-AuNPs adsorb on these binding sites after the addition of BSA-AuNPs, greatly increasing the size and weight of the BSA-AuNP/rGO complex, which leads to clear red precipitates after the 1 h incubation at 65 °C.

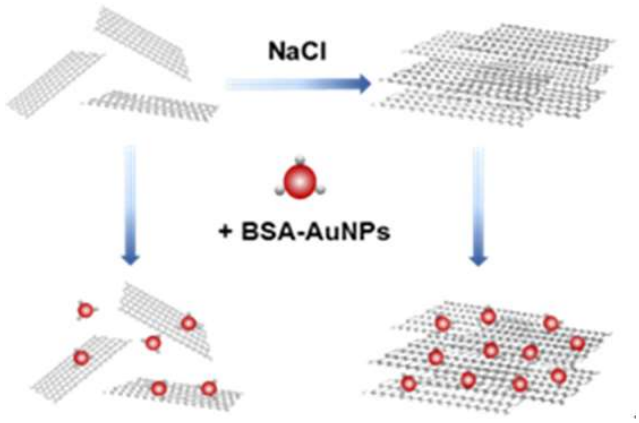

Figure 3.9. Schematic showing the co-precipitation of BSA-AuNPs with aggregated rGO (induced by NaCl) and dispersion of BSA-AuNPs in the presence of unaggregated rGO.

In addition, visible spectra of rGO, BSA-AuNPs, and BSA-AuNPs plus rGO were investigated (Figure 3.10). It is obvious that the spectrum of BSA-AuNPs plus rGO possessed a similar shape to that of BSA-AuNPs alone, with the absorption peak at approximately 528 nm. In the following experiments, the absorbance of the supernatant was detected at 528 nm to analyze the co-precipitation of BSA-AuNPs with rGO. rGO exhibits a weak absorption from 400 to 700 nm.

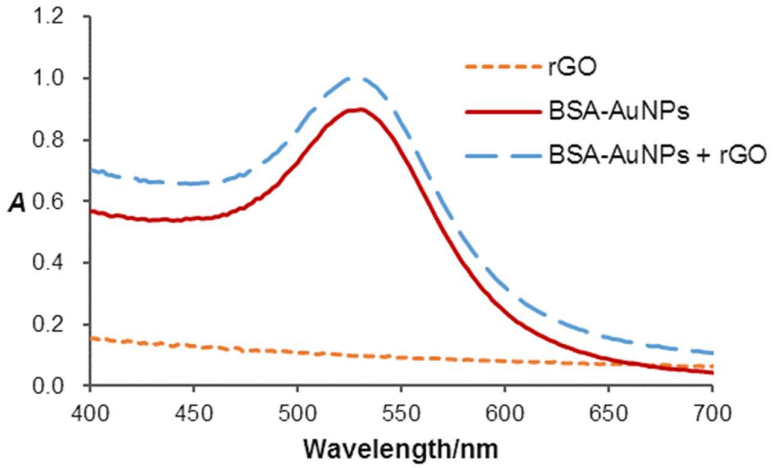

Figure 3.10. Visible spectra of rGO, BSA-AuNPs, and BSA-AuNPs plus rGO mixture. The concentrations of BSA-AuNPs and rGO (if possible) were 2 nM and 8.75 μg mL^{-1}, respectively.

Furthermore, various tests were conducted to optimize the reaction conditions for effective co-precipitation of BSA-AuNPs and rGO. Figure 3.11 shows the effects of different components of reaction buffer on the co-precipitation of BSA-AuNPs with rGO. Aggregation buffer consisted of 20 mM Tris-HCl, 50 mM NaCl, 10 mM $(NH_4)_2SO_4$, and 0.05% Tween 20 (pH 7.4). It can be found that a few red precipitates occurred when rGO was incubated with 50 mM NaCl before the addition BSA-AuNPs, but the precipitation was not effective in terms of easy visual readout. Nevertheless, the aggregation buffer group showed the significantly higher efficiency of the co-precipitation of BSA-AuNPs and rGO, as the supernatant turned almost colorless after incubation at 65 °C. Interestingly, it is also found that 20 mM Tris-HCl, 50 mM NaCl, and 10 mM $(NH_4)_2SO_4$ were not able to lead to the co-precipitation phenomenon alone but contributed to more effective precipitation induced by NaCl. These results showed the effective precipitation could be achieved by using aggregation buffer as the optimal condition.

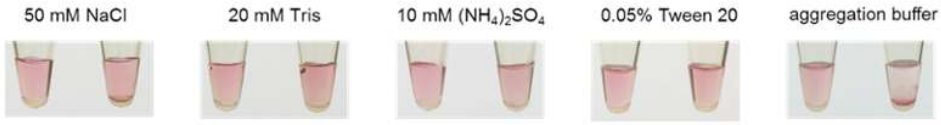

Figure 3.11. Photograph showing the effects of different components of reaction buffer on the co-precipitation of BSA-AuNPs with rGO. rGO were firstly incubated with different components for 1 h at room temperature, followed by the addition of BSA-AuNPs. The photographs were taken after 1 h incubation at 65 °C. Aggregation buffer consists of 20 mM Tris-HCl, 50 mM NaCl, 10 mM $(NH_4)_2SO_4$, and 0.05% Tween 20 (pH 7.4). Samples without rGO were included for comparison. The concentrations of BSA-AuNPs and rGO (if possible) were 2 nM and 8.75 μg mL^{-1}, respectively.

The effect of pH on the co-precipitation of BSA-AuNPs with rGO is presented in Figure 3.12. rGO was firstly incubated with 50 mM NaCl for 1 h at room temperature. After the addition of BSA-AuNPs, the pHs of the reaction mixtures were adjusted, followed by 1 h incubation at 65 °C. The result showed that the precipitation at pH 5 was the most effective among these six pHs, while other pHs (4, 6, 7, 8, and 9) showed about the same precipitation effectiveness according to the absorbance data shown in Figure 3.12 (bottom). It is known that BSA-AuNPs were not stable at pH 5 and precipitated without rGO or NaCl (see Figure 3.7), which indicates the pH 5 should be excluded from consideration for the co-precipitation of BSA-AuNPs and rGO. Besides, as pH from 4 to 9 showed a similar degree of precipitation, it is believed that the aggregation buffer with pH 7.4 is relatively acceptable to achieve an effective precipitation.

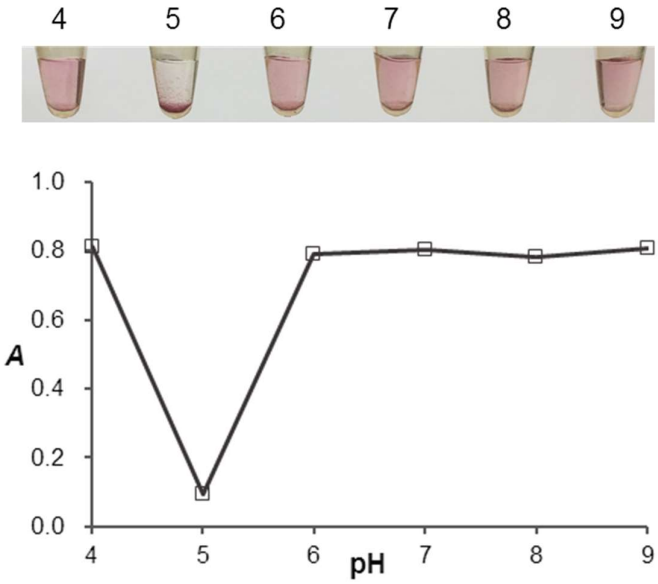

Figure 3.12. (Top) Photograph showing the effect of pH on the co-precipitation of BSA-AuNPs with rGO. rGO was firstly incubated with 50 mM NaCl for 1 h at room temperature. After the addition of BSA-AuNPs, the pHs of the reaction mixtures were adjusted to 4, 5, 6, 7, 8, and 9 by NaOH and HCl, followed by 1 h incubation at 65 °C. The concentrations of BSA-AuNPs and rGO were 2 nM and 8.75 μg mL^{-1}, respectively. (Bottom) Plots of absorbance at 528 nm of supernatant in different pHs (4, 5, 6, 7, 8, and 9).

Moreover, it was found that the rGO concentration had a significant effect on the efficiency of co-precipitation. Various concentrations of rGO were used, and concentration of BSA-AuNPs was kept at 2 nM. As shown in Figure 3.13, after 1 h incubation at 65 °C, an increase of rGO concentration correlated the decrease of absorption intensity of the supernatant of the reaction mixture, which corresponded to the rise of co-precipitation effectiveness. Red precipitates started to appear when rGO concentration was higher than 4.75 μg mL^{-1}. And the effective precipitation could be achieved with rGO at 8.75 and 10.75 μg mL^{-1},

which is easy for visual readout compared with the control sample without rGO. In consideration of cost-effectiveness, 8.75 μg mL^{-1} was chosen as the optimal rGO concentration for the effective co-precipitation of BSA-AuNPs with rGO.

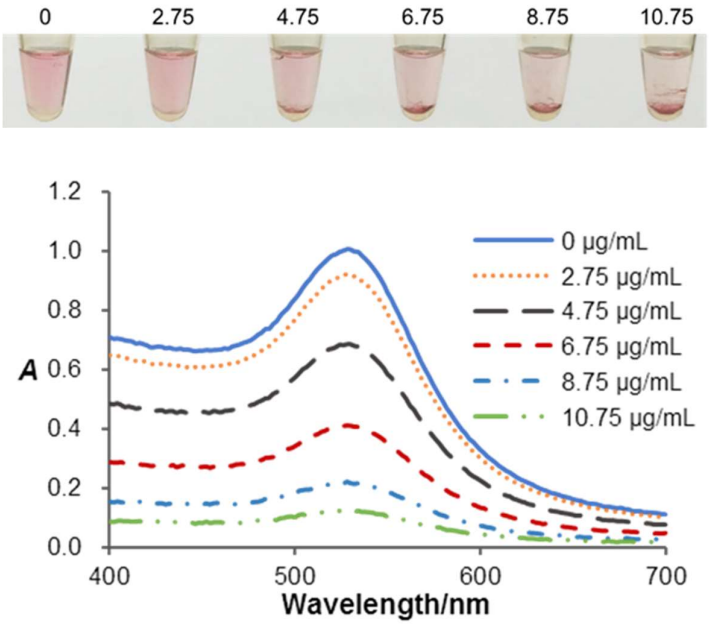

Figure 3.13. (Top) Photograph showing the effect of rGO concentration on the co-precipitation of BSA-AuNPs with rGO. Different concentrations of rGO (0, 2.75, 4.75, 6.75, 8.75, and 10.75 μg mL^{-1}) were firstly incubated with aggregation buffer for 1 h at room temperature. After the addition of BSA-AuNPs, the mixture was incubated at 65 °C for 1 h. The concentration of BSA-AuNPs was 2 nM. (Bottom) Plots of absorbance at 528 nm of supernatant with different concentrations of rGO (0, 2.75, 4.75, 6.75, 8.75, and 10.75 μg mL^{-1}).

The effect of incubation time of rGO in aggregation buffer on the co-precipitation was also studied (shown in Figure 3.14). The results showed that red precipitates could not occur without the incubation of

rGO in aggregation buffer in advance before adding BSA-AuNPs. With incubation time higher than 30 min, an obvious precipitation could be seen by the naked eye. According to the absorption spectra data presented in Figure 1.14 (bottom), the incubation time of 60 min showed nearly the same high co-precipitation effectiveness as 90 and 120 min. In terms of saving detection time and distinct precipitation phenomenon, 60 min was selected as the optimal incubation time of rGO in aggregation buffer.

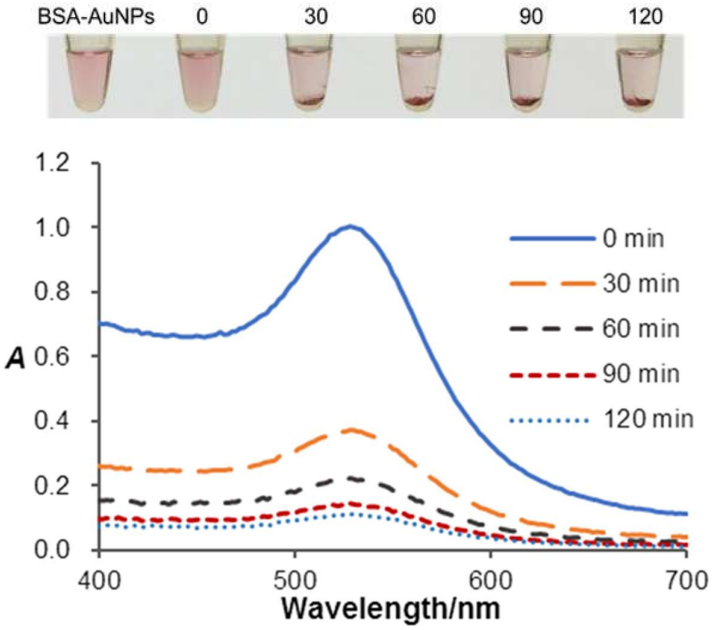

Figure 3.14. (Top) Photograph showing the effect of incubation time of rGO in aggregation buffer on the co-precipitation of BSA-AuNPs with rGO. rGO (8.75 μg mL^{-1}) were firstly incubated with aggregation buffer for different time (0, 30, 60, 90, and 120 min) at room temperature, followed by the addition of BSA-AuNPs. Then the reaction mixture was incubated at 65 °C for 1 h. The concentration of BSA-AuNPs was 2 nM. (Bottom) Absorption spectra of reaction mixtures with different incubation time (0, 30, 60, 90, and 120 min) of rGO in aggregation buffer.

In addition, Figure 3.15 shows the effect of incubation temperature after the addition of BSA-AuNPs on the co-precipitation. It can be found that the absorbance at 528 nm for four temperatures (25, 45, 65, and 85 °C) all decreased over time, which indicated the gradual appearance of precipitation. And an increase of precipitation effectiveness was correlated with the increase of incubation temperature, while the precipitation was similarly effective at 65 °C compared with 85 °C. Besides, for 65 °C, precipitation was found to be efficient within 60 min. Hence, 1 h incubation at 65 °C after the addition of BSA-AuNPs was selected as the optimal condition for the effective precipitation.

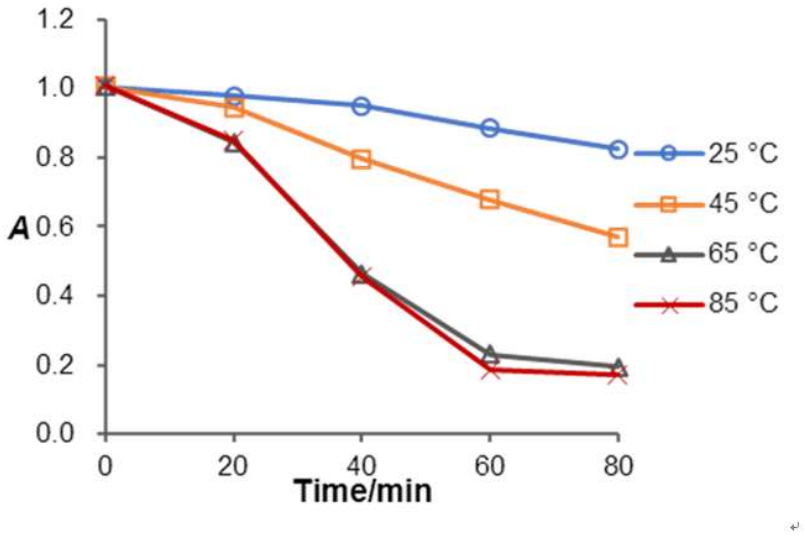

Figure 3.15. Effect of incubation temperature after the addition of BSA-AuNPs on the co-precipitation. rGO (8.75 μg mL^{-1}) was firstly incubated with aggregation buffer for 1 h at room temperature. After the addition of BSA-AuNPs, the mixture was incubated at different temperature (25, 45, 65, and 85 °C). The concentration of BSA-AuNPs was 2 nM. Absorbance values of reaction mixtures at different incubation temperatures (25, 45, 65, and 85 °C) were measured at 528 nm.

Moreover, after the determination of optimal conditions, the effect of BSA concentration in the preparation of BSA-AuNPs on the co-precipitation was investigated. Different concentrations of BSA (0, 1, and 5 mg mL^{-1}) were used in the preparation of BSA-AuNPs and tests were conducted under the optimal conditions. The result shown in Figure 3.16 suggested that all solutions remained dispersed before the incubation at 65 °C. For AuNPs, (that is, 0 mg mL^{-1} BSA), both two tubes (control and BSA-AuNPs plus rGO) were precipitated purple after incubation, which can be explained that the AuNPs could not against the aggregation buffer and the subsequent incubation at 65 °C without the modification of BSA. Compared with BSA-AuNPs with 5 mg mL^{-1} BSA, an effective precipitation occurred after incubation at 65 °C for 1 mg mL^{-1} BSA-AuNPs. It is believed that the excessive BSA could compete with BSA-AuNPs in adsorbing on rGO, which resulted in fewer BSA-AuNPs precipitated with aggregated rGO. These results showed that 1 mg mL^{-1} is the optimal concentration of BSA during the preparation of BSA-AuNPs to achieve an effective precipitation.

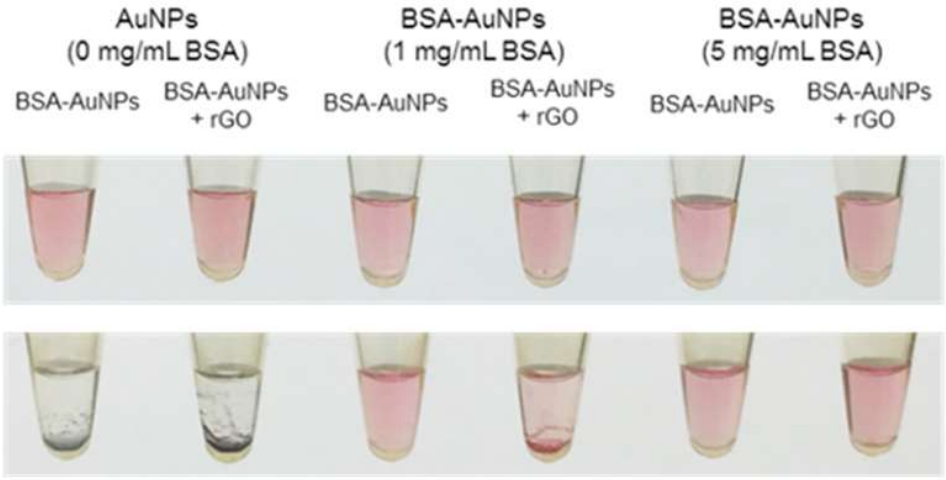

Figure 3.16. Photograph showing the effect of different BSA concentrations (0, 1, and 5 mg mL^{-1}; concentration of AuNPs was fixed at 20 nM) in the preparation of BSA-AuNPs on the co-precipitation of BSA-AuNPs with rGO. The concentrations of BSA-AuNPs and rGO were 2 nM and 8.75 μg mL^{-1}, respectively. The incubation of rGO in aggregation buffer was conducted at room temperature for 1 h, followed by the addition of BSA-AuNPs. The photograph was taken before (top) and after (bottom) the 1 h incubation at 65 °C. Samples without rGO were included for comparison.

3.5. Stabilization Effect of single-stranded DNA (ssDNA) on rGO

It is found that the aggregation of rGO could be induced by the aggregation buffer, and subsequently led to the co-precipitation with BSA-AuNPs. One efficient way to protect rGO from salt-induced aggregation is by the stabilization effect of single-stranded DNA (ssDNA). The binding of ssDNA to rGO through π-stacking interaction renders additional negative charge, thus allowing rGO to remain dispersed at high salt concentrations. As shown in Figure 3.17, the

stabilization effect raised linearly with increasing ssDNA concentration up to 100 nM. At higher ssDNA concentrations, the curve remained level due to the saturation of ssDNA on the rGO. However, double-stranded DNA (dsDNA) was not capable of stabilizing rGO from aggregation. Thereby obvious precipitation appeared regardless of the concentration of dsDNA (0–150 nM). Furthermore, DLS analysis was carried out for demonstrating the stabilization of ssDNA (Figure 3.18). It is found that after 1 h incubation in aggregation buffer, the average size of rGO turned out to be 1340.6 nm, which indicated the significant aggregation of rGO compared with initial size after reduction and redispersion, 238.7 nm (presented in Figure 3.4). In the presence of 100 nM ssDNA, the average size of rGO was determined to be 298.9 nm, close to the initial size of rGO, which shows the effective stabilization effect of ssDNA. And the average size of rGO with 100 nM dsDNA after 1 h incubation in aggregation buffer changed to 1281.3 nm, verifying that dsDNA was not able to protect rGO from salt-induced aggregation. Thus, the size was tolerably same to that of rGO without DNA.

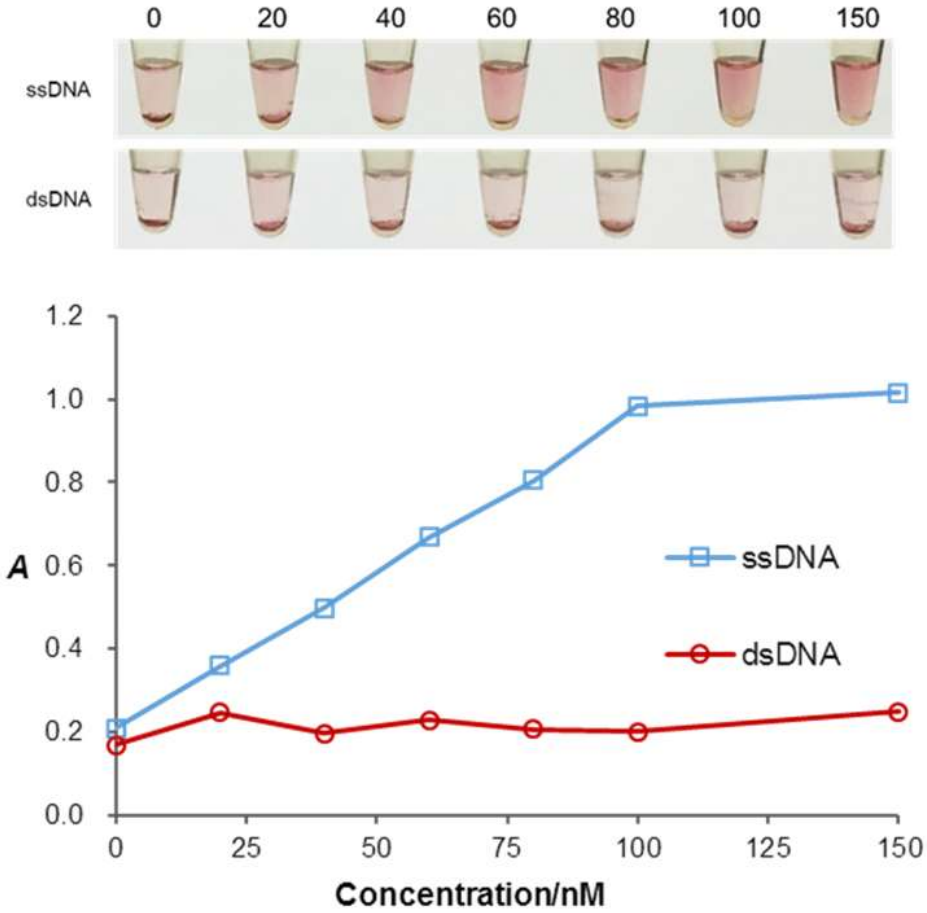

Figure 3.17. Stabilization effects of single-stranded DNA (ssDNA) on rGO compared with double-stranded DNA (dsDNA). (Top) Photograph showing the co-precipitation of BSA-AuNPs with rGO in the presence of different concentrations (0, 20, 40, 60, 80,100, and 150 nM) of ssDNA (top) or dsDNA (bottom). The concentrations of BSA-AuNPs and rGO were 2 nM and 8.75 μg mL^{-1}, respectively. The incubation of rGO in aggregation buffer was carried out for 1 h at room temperature, followed by the addition of BSA-AuNPs. The photograph was taken after 1 h incubation at 65 °C. (Bottom) Plots of absorbance at 528 nm versus concentrations of DNA of samples in (top).

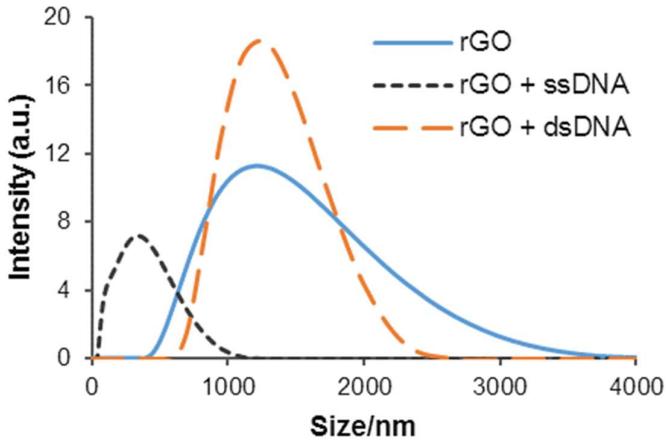

Figure 3.18. DLS analysis of rGO, rGO with 100 nM single-stranded DNA (ssDNA), and rGO with 100 nM double-stranded DNA (dsDNA) after 1 h incubation in aggregation buffer at room temperature. The concentration of rGO was 10 μg mL^{-1}.

3.6. Precipitation-Based Detection of Oligonucleotide Target Using BSA-AuNPs and rGO

Taking advantage of ssDNA-controlled and salt-induced aggregation property as well as the co-precipitation of BSA-AuNPs with rGO, we developed a simple precipitation-based detection platform using BSA-AuNPs and rGO for oligonucleotide target. Without the target, BSA-AuNPs should remain dispersed due to the stabilization effect of single-stranded probes on rGO from salt-induced aggregation. While in the presence of the target DNA, the double-stranded hybrids are not able to protect rGO from salt-induced aggregation. Thus, BSA-AuNPs exhibit rapid co-precipitation with aggregated rGO. In the precipitation-based detection of oligonucleotide target, rGO (8.75 μg mL^{-1}) was first incubated with probe sequence (100 nM) as well as different concentrations of target DNA sequence (0–100 nM) in aggregation

buffer at room temperature for 1 h, followed by the addition of BSA-AuNPs (2 nM). The mixture of BSA-AuNPs and rGO was then incubated at 65 °C for 1 h. After that, the absorbance of the supernatant was measured at 528 nm. As expected, the degree of precipitation increased linearly with the increase of target concentration (shown in Figure 3.19). Plots of absorbance at 528 nm versus concentration of target DNA are also presented. The limit of detection based on three times the standard deviation of the blank was determined to be 5 nM, which compared favorably with previous reported precipitation-based work [71].

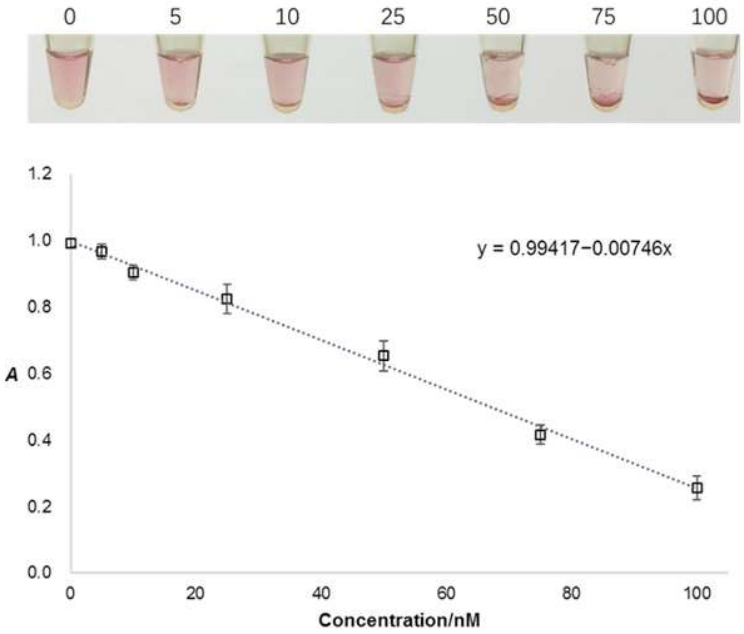

Figure 3.19. (Top) Photograph showing the detection of different concentrations of target DNA sequence (0–100 nM). (Bottom) Plots of absorbance at 528 nm for samples in (top). The optimal conditions for effective co-precipitation of BSA-AuNPs and rGO were used in detection. The concentrations of BSA-AuNPs and rGO were 2 nM and 8.75 μg mL^{-1}, respectively. Error bars were obtained from three parallel experiments.

3.7. Precipitation-Based Detection of PCR and HDA Products Using BSA-AuNPs and rGO

Furthermore, to achieve high detection sensitivity, we utilized the platform for polymerase chain reaction (PCR) and helicase-dependent amplification (HDA) product detection. In amplification reaction product detection, as the primers for amplification were used for stabilizing rGO instead of 29-base ssDNA probes, the stabilization effects of PCR primers (22 bases) and HDA primers (27 bases) were studied firstly under identical conditions. As shown in Figure 3.20, a decrease of precipitation effect correlated with the increase of the concentration of primers. The suitable concentrations of primers for HDA and PCR product detection were 100 and 400 nM, respectively.

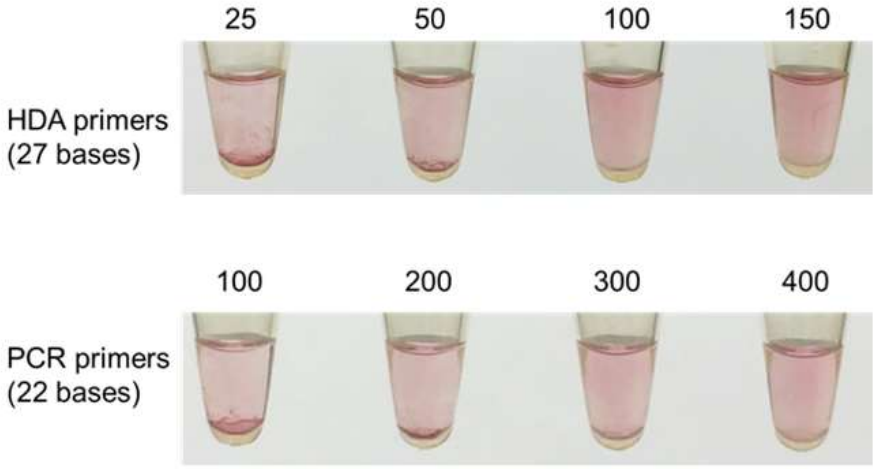

Figure 3.20. Photograph showing the stabilization effects of PCR and HDA primers on rGO (unit: nM). The concentrations of BSA-AuNPs and rGO were 2 nM and 8.75 μg mL^{-1}, respectively. The incubation of rGO in aggregation buffer was carried out for 1 h at room temperature, followed by the addition of BSA-AuNPs. The photograph was taken after 1 h incubation at 65 °C.

Then, we used the precipitation-based platform for PCR product detection. The PCR samples (3-fold dilution, unpurified sample, *i.e.,* without any kind of post-PCR cleanup of enzymes and dNTPs) were added to rGO. Subsequent experiments were identical to those for the 29-base oligonucleotide target. As shown in Figure 3.21, without target (ΦX174 DNA in this case), BSA-AuNPs remained dispersed due to the stabilization effect of single-stranded probes on rGO from salt-induced aggregation. While in the presence of the target ΦX174 DNA, the double-stranded PCR products were not able to protect rGO from salt-induced aggregation, thus BSA-AuNPs exhibited rapid co-precipitation with aggregated rGO. Therefore, for the negative sample, reaction mixture remained dispersed, while a clearly distinguishable precipitation appeared in the presence of target. For specificity test, the sample containing the nonspecific template (lambda DNA, 10^7 copies) remained as a red dispersion, like the sample with only UltraPure water. Besides, the samples containing only the specific template as well as both the specific and nonspecific templates showed obvious red precipitates. For sensitivity test, different copies of ΦX174 DNA (0,10^3, 10^4, 10^5, 10^6, and 10^7 copies) were used for PCR. Results showed that a few red precipitates appeared with 10^6 copies of target ΦX174 DNA and clear precipitation appeared with 10^7 copies. The detection for PCR product using BSA-AuNPs and rGO possess high specificity, and the limit of detection combined with PCR is 10^6 copies (equivalent to 83 fM), which showed the sensitivity for nucleic acid detection had been significantly improved compared to the detection of oligonucleotide target.

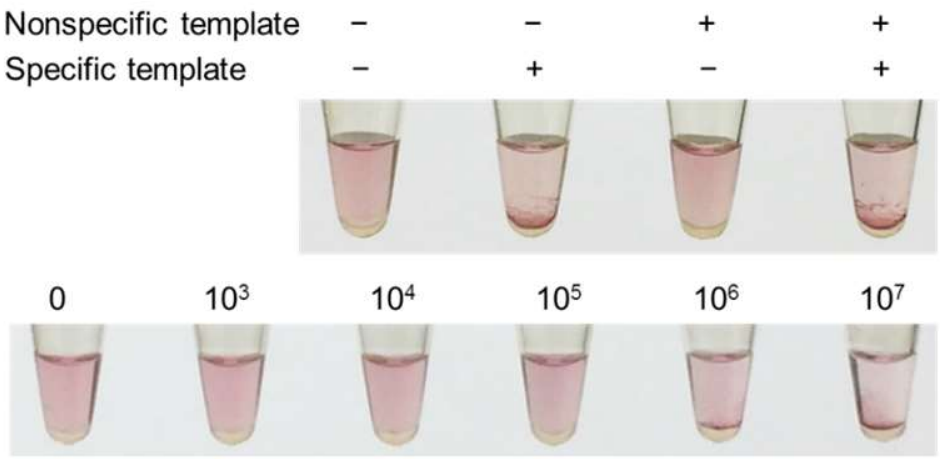

Figure 3.21. Specificity and sensitivity of the detection of PCR product using BSA-AuNPs and rGO. The PCR products were diluted by 3-fold, and other conditions were identical to those optimized for efficient co-precipitation of BSA-AuNPs with rGO. (Top) Photograph showing the detection results of PCR product with four different template combinations of ΦX174 DNA (specific template) and Lambda DNA (nonspecific template): (from left to right) sample without template, sample with ΦX174 DNA, sample with lambda DNA, and sample with ΦX174 DNA and lambda DNA. The copy number of both templates was 10^7. (Bottom) Photograph showing the detection of PCR product with different copy numbers of ΦX174 target: (from left to right) 0,10^3, 10^4, 10^5, 10^6, and 10^7 copies.

In addition, the amplification results of specificity and sensitivity tests were confirmed by agarose gel electrophoresis (shown in Figure 3.22). As expected, a band appeared at around 150 bp (amplicon size: 151 bp) in the samples containing specific ΦX174 DNA in specificity test and in the samples with number of target DNA higher than 10^4 copies in the sensitivity test. This result indicated that successful DNA amplification was achieved. Besides, an increase of band intensity was correlated with increasing copies of the ΦX174 template, suggesting that more

target could lead to more amplicons in PCR.

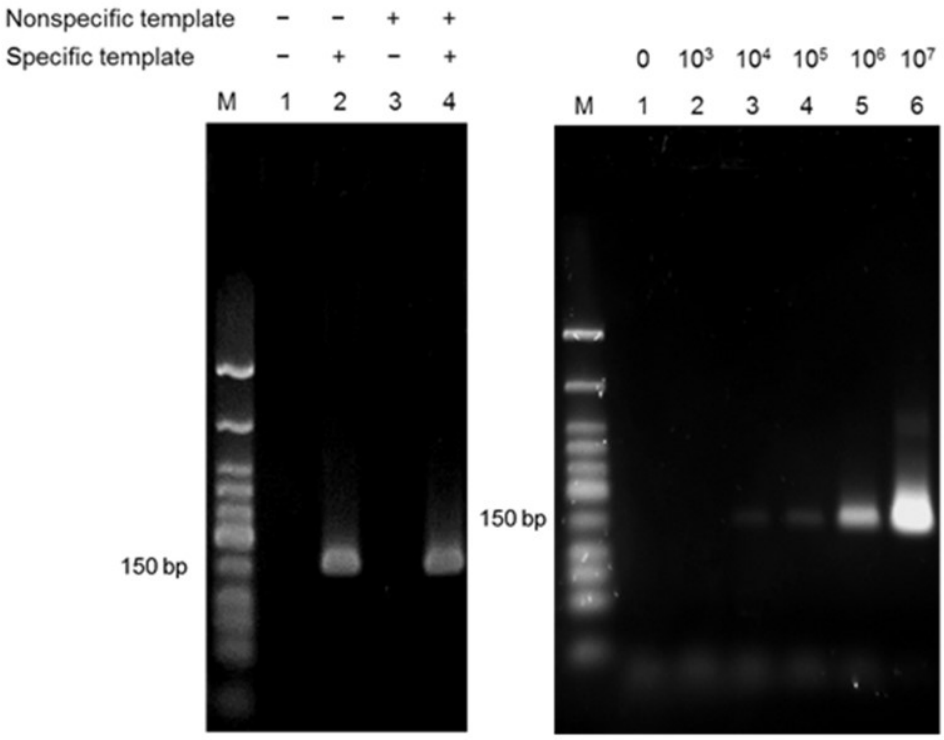

Figure 3.22. Agarose gel electrophoresis results showing the specificity (left) and sensitivity (right) of PCR. Lane M: DNA ladder. (Left) Electropherogram showing the PCR results with four different template combinations of ΦX174 DNA (specific template) and Lambda DNA (nonspecific template): (from lane 1 to lane 4) sample without template, sample with ΦX174 DNA, sample with lambda DNA, and sample with ΦX174 DNA and lambda DNA. The copy number of both templates was 10^7. (Right) Electropherogram showing the PCR results with different copy numbers of ΦX174 target: (from lane 1 to lane 6) 0, 10^3, 10^4, 10^5, 10^6, and 10^7 copies.

Besides, we utilized the precipitation-based platform for HDA product detection. Similar to the PCR product detection, the HDA samples (4-fold dilution, unpurified sample) were added to rGO, followed by the

incubation in aggregation buffer. Subsequent experiments were identical to those for the 29-base oligonucleotide target. As shown in Figure 3.23, without target (pCNG1 DNA in this case), BSA-AuNPs remained dispersed, while in the presence of the target pCNG1 DNA, the double-stranded HDA products could not protect rGO from salt-induced aggregation. Thus, BSA-AuNPs exhibited rapid co-precipitation with aggregated rGO (red precipitates). For specificity test, the sample containing the nonspecific template (Lambda DNA, 500000 copies) remained as a red dispersion, like the sample with only UltraPure water. Besides, the sample containing only the specific template as well as both the specific and nonspecific templates showed obvious red precipitates. For sensitivity test, various copies of pCNG1 DNA (0, 50, 500, 5000, 50000, and 50000 copies) were used for HDA. Results showed that red precipitates appeared with more than 500 copies of pCNG1 DNA and effective precipitation happened with the same copies. The detection combined with HDA also showed significantly high specificity. Moreover, the detection of HDA product could achieve obvious precipitation with only 500 copies of target DNA (equivalent to 21 aM), showing higher sensitivity than the detection of PCR product.

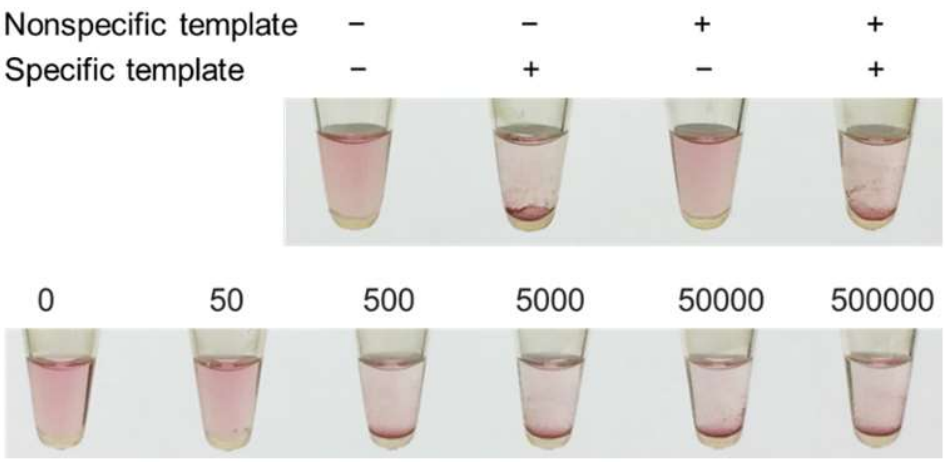

Figure 3.23. Specificity and sensitivity of the detection of HDA product using BSA-AuNPs and rGO. The HDA products were diluted by 4-fold, and other conditions were identical to those optimized for efficient co-precipitation of BSA-AuNPs with rGO. (Top) Photograph showing the detection results of HDA product with four different template combinations of pCNG1 DNA (specific template) and Lambda DNA (nonspecific template): (from left to right) sample without template, sample with pCNG1 DNA, sample with lambda DNA, and sample with pCNG1 DNA and lambda DNA. The copy number of both templates was 500000. (Bottom) Photograph showing the detection of HDA product with different copy numbers of pCNG1 target: (from left to right) 0,50, 500, 5000, 50000, and 500000 copies.

Also, the amplification results of specificity and sensitivity tests were confirmed by agarose gel electrophoresis (shown in Figure 3.24). As expected, a band appeared at around 100 bp (HDA amplicon size: 102 bp) in the samples containing specific pCNG1 DNA in specificity test and the samples with number of target DNA higher than 500 copies in sensitivity test. This result indicated that successful HDA reaction was achieved. As the intensities of bands with different copies were almost

the same, it is believed that HDA could be efficient so long as the copy number is beyond the minimum limit to initialize the amplification.

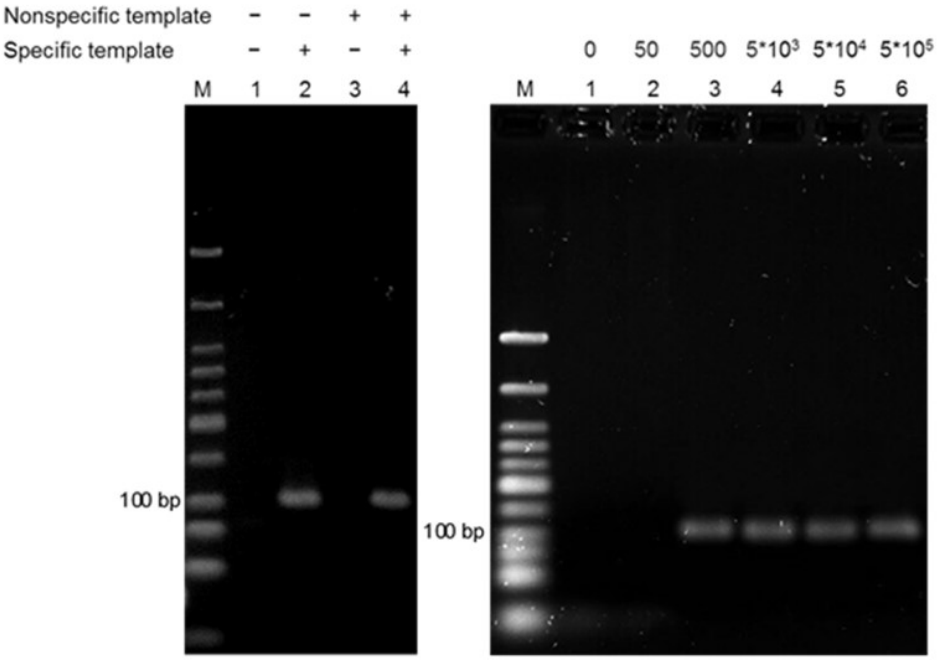

Figure 3.24. Agarose gel electrophoresis results showing the specificity (left) and sensitivity (right) of HDA. Lane M: DNA ladder. (Left) Electropherogram showing the HDA reactions with four different template combinations of pCNG1 DNA (specific template) and Lambda DNA (nonspecific template): (from lane 1 to lane 4) sample without template, sample with pCNG1 DNA, sample with lambda DNA, and sample with pCNG1 DNA and lambda DNA. The copy number of both templates was 500000. (Right) Electropherogram showing the HDA reactions with different copy numbers of pCNG1 target: (from lane 1 to lane 6) 0, 50, 500, 5000, 50000, and 500000 copies.

Chapter 4 Conclusions and Recommendations for Future Work

4.1. Conclusions

The detection of nucleic acid plays an increasingly significant role in various fields, including medical diagnosis, food safety testing, and biowarfare agent detection. In recent years, great emphasis is placed on decentralized testing in resource-limited settings. One crucial requirement is simple recognition readout. As color readout by the naked eye is ideally suited for this purpose, gold nanoparticles have been widely used in colorimetric detection due to their unique optical properties. Typical assays involve the use of oligonucleotide-modified gold nanoparticles. However, it should be noted that oligonucleotide-modified gold nanoparticles are prepared using thiol-modified oligonucleotides, which means high cost. Besides, it should be pointed that the red and purple color can sometimes be difficult to differentiate by the naked eye. An immense potential has also been shown to combine the detection with nucleic acid amplification to achieve the ultrasensitive detection platforms, whereas only a few of the related work has been reported due to the lack of effective detection strategies.

In this study, to address these drawbacks, we developed a simple precipitation-based nucleic acid detection platform using BSA-AuNPs and rGO. BSA-AuNP exhibited the lowest stability at pH 5 and rGO was found to more sensitive to salt-induced aggregation than GO. The co-precipitation only appeared when BSA-AuNPs were mixed with aggregated rGO. Besides, the optimal conditions for effective

precipitation phenomenon were determined (*i.e.*, rGO was incubated in aggregation buffer at room temperature for 1 h, followed by the addition of BSA-AuNPs and subsequent 1 h incubation at 65 °C; The concentrations of BSA-AuNPs and rGO were 8.75 μg mL $^{-1}$ and 2 nM, respectively). For DNA detection, without the target, BSA-AuNPs remained dispersed due to the stabilization effect of single-stranded probes on rGO from salt-induced aggregation. While in the presence of the target DNA, the double-stranded hybrids could not protect rGO, hence red precipitates appeared due to the co-precipitation of BSA-AuNPs with aggregated rGO. The range and the limit of detection for oligonucleotide target were 5–100 nM and 5 nM, respectively. Moreover, to achieve ultrasensitive platform, we utilized this precipitation-based platform for PCR and HDA product detection. Combined with PCR, clear red precipitates could be observed in the sample with 10^6 copies (equivalent to 83 fM). And the sensitivity of this platform was further improved to 500 copies (21 aM) with HDA. This precipitation-based platform has the advantages of low cost and simple preparation due to the use of BSA-AuNPs instead of conventional oligo-AuNPs. Besides, precipitation is more suitable for the requirement of easy readout compared with the color change. The combination of the detection with HDA (isothermal amplification reaction) shows the advantages of ultrasensitive performance and simple temperature control. This platform is well suited for decentralized testing and, to the best of our knowledge, is the first attempt utilizing the co-precipitation of BSA-AuNPs with rGO for nucleic acid detection.

4.2. Recommendations for Future Work

Based on the new detection mechanism developed in this study, several further investigations can be carried out to widen the applications as well as improve the performance of this precipitation-based platform. Firstly, the phenomenon that precipitation occurred only when BSA-AuNPs were incubated with aggregated rGO can be further explored. For instance, the chemical explanation of the co-precipitation should be given. Other parameters which may have potential to affect the efficiency of precipitation need to be studied, such as the concentration of BSA-AuNPs, reduction degree of rGO, and type of surfactant. Secondly, this universal platform successfully combined both thermal amplification reaction (PCR in this case) and isothermal method (HDA) with detection. However, the applicability for other kinds of amplification reactions needs to be investigated. Utilizing other kinds of nucleic acid amplification strategies may also be possible to achieve higher sensitivity. Thirdly, successful HDA was achieved with only 500 copies of the specific template in this study. Nevertheless, the detection for PCR product showed less sensitive performance as the number of specific templates should reach 10^4. As a successful PCR was demonstrated with only 1 copy of target, we believe that the sensitivity of our precipitation-based assay for PCR product can be further improved by optimizing the PCR conditions. Finally, single-stranded DNA probes were used to stabilize rGO from salt-induced aggregation, and double-stranded hybrids could not protect rGO, which resulted in a difference between negative and positive samples. With the same principle, it is believed that by using aptamer, this platform is greatly possible to a broad spectrum of non-nucleic acid targets, such as ions,

proteins, and small molecules.

References

[1] Niemz, A., Ferguson, T.M., Boyle, D.S., Point-of-care nucleic acid testing for infectious diseases. *Trends Biotechnol.* 2011, *29*, 240–250.

[2] Saiki, R.K., Gelfand, D.H., Stoffel, S., Scharf, S.J., Higuchi, R., Horn, G.T., Mullis, K.B., Erlich, H.A., Primer-directed enzymatic amplification of DNA with a thermostable DNA polymerase, *Science* 1988, *239*, 487–491.

[3] Pusterla, N., Madigan, J.E., Leutenegger, C.M., Real-time polymerase chain reaction: a novel molecular diagnostic tool for equine infectious diseases. *J. Vet. Intern. Med.* 2006, *20*, 3–12.

[4] Bustin, S.A., Absolute quantification of mRNA using real-time reverse transcription polymerase chain reaction assays. *J. Mol. Endocrinol.* 2000, *25*, 169–193.

[5] Ririe, Kirk M., Rasmussen, Randy P., Witter, C.T., Product differentiation by analysis of DNA melting curves during the polymerase chain reaction. *Anal. Biochem.* 1997, *245*, 154–160.

[6] Heid, C.A., Stevens, J., Livak, K.J., Williams, P.M., Real time quantitative PCR. *Genome Res.* 1996, *6*, 986–994.

[7] Craw, P., Balachandran, W., Isothermal nucleic acid amplification technologies for point-of-care diagnostics: a critical review. *Lab Chip* 2012, *12*, 2469–2486.

[8] Jean, J., D'Souza, D.H., Jaykus, L.A., Multiplex nucleic acid sequence-based amplification for simultaneous detection of several enteric viruses in model ready-to-eat foods. *Appl. Environ. Microbiol.* 2004, *70*, 6603–6610.

[9] Notomi, T., Okayama, H., Masubuchi, H., Yonekawa, T., Watanabe, K., Amino, N., Hase, T., Loop-mediated isothermal amplification of DNA.

Nucleic Acids Res. 2000, *28*, E63.

[10] Vincent, M., Xu, Y., Kong, H., Helicase-dependent isothermal DNA amplification. *EMBO Rep.* 2004, *5*, 795–800.

[11] Compton, J., Nucleic acid sequence-based amplification. *Nature* 1991, *350*, 91–92.

[12] Uemori, T., Mukai, H., Takeda, O., Moriyama, M., Sato, Y., Hokazono, S., Takatsu, N., Asada, K., Kato, I., Investigation of the molecular mechanism of ICAN, a novel gene amplification method. *J. Biochem.* 2007, *142*, 283–292.

[13] L. Zhang, F. X. Gu, J. M. Chan, A. Z. Wang, R. S. Langer, O. C. Farokhzad, Nanoparticles in medicine: Therapeutic applications and developments, Clin. Pharmacol. Ther., 2008, 83, 761–769.

[14] Dreaden, E.C., Alkilany, A.M., Huang, X., Murphy, C.J., El-Sayed, M.A., The golden age: gold nanoparticles for biomedicine. *Chem. Soc. Rev.* 2012, *41*, 2740–2779.

[15] Daniel, M.C.M., Astruc, D., Gold nanoparticles: Assembly, supramolecular chemistry, quantum-size related properties and applications toward biology, catalysis and nanotechnology. *Chem. Rev.* 2004, *104*, 293–346.

[16] Turkevich, J., Stevenson, P.C., Hiller, J., A study of the nucleation and growth processes in the synthesis of colloidal gold. *Discuss. Faraday Soc.* 1951, *11*, 55–75.

[17] Zhao, W., Brook, M.A., Li, Y., Design of gold nanoparticle-based colorimetric biosensing assays. *ChemBioChem* 2008, *9*, 2363–2371.

[18] Kelly, K.L., Coronado, E., Zhao, L.L., Schatz, G.C., The optical properties of metal nanoparticles: The influence of size, shape, and dielectric environment. *J. Phys. Chem. B* 2003, *107*, 668–677.

[19] http://www.cytodiagnostics.com/gold_nanoparticle_properties.php.

[20] Mirkin, C.A., Letsinger, R.L., Mucic, R.C., Storhoff, J.J., A DNA-based method for rationally assembling nanoparticles into macroscopic materials. *Nature* 1996, *382*, 607–609.

[21] Giljohann, D.A., Seferos, D.S., Daniel, W.L., Massich, M.D., Patel, P.C., Mirkin, C.A., Gold nanoparticles for biology and medicine. *Angew. Chemie - Int. Ed.* 2010, *49*, 3280–3294.

[22] Hlady, V., Buijs, J., Protein adsorption on solid surfaces. *Curr. Opin. Biotechnol.* 1996, *7*, 72–77.

[23] Brorson, S.H., Bovine serum albumin (BSA) as a reagent against non-specific immunogold labeling on LR-white and epoxy resin. *Micron* 1997, *28*, 189–195.

[24] Xiao, Y., Isaacs, S.N., Enzyme-linked immunosorbent assay (ELISA) and blocking with bovine serum albumin (BSA)-not all BSAs are alike. *J. Immunol. Methods* 2012, *384*, 148–151.

[25] Wang, X.X., Wu, Q., Shan, Z., Huang, Q.M., BSA-stabilized Au clusters as peroxidase mimetics for use in xanthine detection. *Biosens. Bioelectron.* 2011, *26*, 3614–3619.

[26] Brewer, S.H., Glomm, W.R., Johnson, M.C., Knag, M.K., Franzen, S., Probing BSA binding to citrate-coated gold nanoparticles and surfaces. *Langmuir* 2005, *21*, 9303 – 9307.

[27] Wong, J.K.F., Yip, S.P., Lee, T.M.H., Silica-modified oligonucleotide-gold nanoparticle conjugate enables closed-tube colorimetric polymerase chain reaction. *Small* 2012, *8*, 214–219.

[28] Fu, R., Wang, C., Zhuang, J., Yang, W., Adsorption and desorption of DNA on bovine serum albumin modified gold nanoparticles. *Colloids Surfaces A Physicochem. Eng. Asp.* 2014, *444*, 326–329.

[29] Elghanian, R., Storhoff, J.J., Mucic, R.C., Letsinger, R.L., Mirkin, C.A., Selective colorimetric detection of polynucleotides based on the

distance-dependent optical properties of gold nanoparticles. 1997, *277*.

[30] Storhoff, J.J., Elghanian, R., Mucic, R.C., Mirkin, C.A., Letsinger, R.L., One-pot colorimetric differentiation of polynucleotides with single base imperfections using gold nanoparticle probes. *J. Am. Chem. Soc.* 1998, *120*, 1959–1964.

[31] Sato, K., Hosokawa, K., Maeda, M., Rapid aggregation of gold nanoparticles induced by non-cross-linking DNA hybridization. *J. Am. Chem. Soc.* 2003, *125*, 8102–8103.

[32] Baptista, P., Doria, G., Henriques, D., Pereira, E., Franco, R., Colorimetric detection of eukaryotic gene expression with DNA-derivatized gold nanoparticles. *J. Biotechnol.* 2005, *119*, 111–117.

[33] Li, H., Rothberg, L., Colorimetric detection of DNA sequences based on electrostatic interactions with unmodified gold nanoparticles. *Proc. Natl. Acad. Sci. U. S. A.* 2004, *101*, 14036–9.

[34] Sato, K., Hosokawa, K., Maeda, M., Non-cross-linking gold nanoparticle aggregation as a detection method for single-base substitutions. *Nucleic Acids Res.* 2005, *33*.

[35] Jung, Y.L., Jung, C., Parab, H., Li, T., Park, H.G., Direct colorimetric diagnosis of pathogen infections by utilizing thiol-labeled PCR primers and unmodified gold nanoparticles. *Biosens. Bioelectron.* 2010, *25*, 1941–1946.

[36] Deng, H., Xu, Y., Liu, Y., Che, Z., Guo, H., Shan, S., Sun, Y., Liu, X., Huang, K., Ma, X., Wu, Y., Liang, X.J., Gold nanoparticles with asymmetric polymerase chain reaction for colorimetric detection of DNA sequence. *Anal. Chem.* 2012, *84*, 1253–1258.

[37] Gill, P., Alvandi, A.H., Abdul-Tehrani, H., Sadeghizadeh, M., Colorimetric detection of Helicobacter pylori DNA using isothermal helicase-dependent amplification and gold nanoparticle probes. *Diagn.*

Microbiol. Infect. Dis. 2008, *62*, 119–124.

[38] Cui, L., Ke, G., Zhang, W.Y., Yang, C.J., A universal platform for sensitive and selective colorimetric DNA detection based on Exo III assisted signal amplification. *Biosens. Bioelectron.* 2011, *26*, 2796–2800.

[39] Song, J., Li, Z., Cheng, Y., Liu, C., Self-aggregation of oligonucleotide-functionalized gold nanoparticles and its applications for highly sensitive detection of DNA. *Chem. Commun.* 2010, *46*, 5548.

[40] Mollasalehi, H., Yazdanparast, R., Non-crosslinking gold nanoprobes for detection of nucleic acid sequence-based amplification products. *Anal. Biochem.* 2012, *425*, 91–95.

[41] Seetang-Nun, Y., Jaroenram, W., Sriurairatana, S., Suebsing, R., Kiatpathomchai, W., Visual detection of white spot syndrome virus using DNA-functionalized gold nanoparticles as probes combined with loop-mediated isothermal amplification. *Mol. Cell. Probes* 2013, *27*, 71–79.

[42] Arunrut, N., Kampeera, J., Sirithammajak, S., Sanguanrut, P., Proespraiwong, P., Suebsing, R., Kiatpathomchai, W., Sensitive visual detection of AHPND bacteria using loop-mediated isothermal amplification combined with DNAFunctionalized gold nanoparticles as probes. *PLoS One* 2016, *11*, 1–18.

[43] Zhou, C., Mu, Y., Yang, M., Wu, Q., Xu, W., Zhang, Y., Jin, W., Song, Q., Wu, Z., Jin, Q., Gold nanoparticles based colorimetric detection of target DNA after loop-mediated isothermal amplification. *Chem. Res. Chinese Univ.* 2013, *29*, 424–428.

[44] Gao, W., The chemistry of graphene oxide. *Graphene Oxide Reduct. Recipes, Spectrosc. Appl.* 2015, 61–95.

[45] Lee, B.S., Lee, Y., Hwang, J.Y., Choi, Y.C., Structural properties of reduced graphene oxides prepared using various reducing agents.

Carbon Lett. 2015, *16*, 255–259.

[46] Hummers, W.S., Offeman, R.E., Preparation of graphitic oxide. *J. Am. Chem. Soc.* 1958, *80*, 1339–1339.

[47] Stankovich, S., Dikin, D.A., Piner, R.D., Kohlhaas, K.A., Kleinhammes, A., Jia, Y., Wu, Y., Nguyen, S.B.T., Ruoff, R.S., Synthesis of graphene-based nanosheets via chemical reduction of exfoliated graphite oxide. *Carbon N. Y.* 2007, *45*, 1558–1565.

[48] Li, B., Cao, X., Ong, H.G., Cheah, J.W., Zhou, X., Yin, Z., Li, H., Wang, J., Boey, F., Huang, W., Zhang, H., All-carbon electronic devices fabricated by directly grown single-walled carbon nanotubes on reduced graphene oxide electrodes. *Adv. Mater.* 2010, *22*, 3058–3061.

[49] Hu, W., Peng, C., Luo, W., Lv, M., Li, X., Li, D., Huang, Q., Fan, C., Graphene-based antibacterial paper. *ACS Nano* 2010, *4*, 4317–4323.

[50] Yin, Z.Y., Sun, S.Y., Salim, T., Wu, S.X., Huang, X.A., He, Q.Y., Lam, Y.M., Zhang, H., Organic photovoltaic devices using highly flexible reduced graphene oxide films as transparent electrodes. *ACS Nano* 2010, *4*, 5263–5268.

[51] Wang, Y., Shi, Z., Huang, Y., Ma, Y., Wang, C., Chen, M., Chen, Y., Supercapacitor devices based on graphene materials.pdf. *J. Phys. Chem. C* 2009, *113*, 13103–13107.

[52] Fan, X., Peng, W., Li, Y., Li, X., Wang, S., Zhang, G., Zhang, F., Deoxygenation of exfoliated graphite oxide under alkaline conditions: a green route to graphene preparation. *Adv. Mater.* 2008, *20*, 4490–4493.

[53] Abulizi, A., Okitsu, K., Zhu, J.J., Bo, Z., Shuai, X., Mao, S., Yang, H., Qian, J., Chen, J.J.-T.J., Yan, J., Cen, K., Fernández-Merino, M.J., Guardia, L., Paredes, J.I., Villar-Rodil, S., Solís-Fernández, P., Martí nez-Alonso, A., Tascón, J.M.D., Vitamin C is an ideal substitute for hydrazine in the reduction of graphene oxide suspensions. *J. Phys.*

Chem. C 2013, *4*, 6426–6432.

[54] Shin, H.J., Kim, K.K., Benayad, A., Yoon, S.M., Park, H.K., Jung, I.S., Jin, M.H., Jeong, H.K., Kim, J.M., Choi, J.Y., Lee, Y.H., Efficient reduction of graphite oxide by sodium borohydride and its effect on electrical conductance. *Adv. Funct. Mater.* 2009, *19*, 1987–1992.

[55] Wu, M., Kempaiah, R., Huang, P.J.J., Maheshwari, V., Liu, J., Adsorption and desorption of DNA on graphene oxide studied by fluorescently labeled oligonucleotides. *Langmuir* 2011, *27*, 2731–2738.

[56] Wu, L., Liu, L., Gao, B., Muñoz-Carpena, R., Zhang, M., Chen, H., Zhou, Z., Wang, H., Aggregation kinetics of graphene oxides in aqueous solutions: Experiments, mechanisms, and modeling. *Langmuir* 2013, *29*, 15174–15181.

[57] Wang, Y., Li, Z., Wang, J., Li, J., Lin, Y., Graphene and graphene oxide: Biofunctionalization and applications in biotechnology. *Trends Biotechnol.* 2011, *29*, 205–212.

[58] Lu, C.H., Yang, H.H., Zhu, C.L., Chen, X., Chen, G.N., A graphene platform for sensing biomolecules. *Angew. Chemie - Int. Ed.* 2009, *48*, 4785–4787.

[59] Park, J.S., Na, H.-K., Min, D.-H., Kim, D.-E., Desorption of single-stranded nucleic acids from graphene oxide by disruption of hydrogen bonding. *Analyst* 2013, *138*, 1745.

[60] He, S., Song, B., Li, D., Zhu, C., Qi, W., Wen, Y., Wang, L., Song, S., Fang, H., Fan, C., A graphene nanoprobe for rapid, sensitive, and multicolor fluorescent DNA analysis. *Adv. Funct. Mater.* 2010, *20*, 453–459.

[61] Li, F., Huang, Y., Yang, Q., Zhong, Z., Li, D., Wang, L., Song, S., Fan, C., A graphene-enhanced molecular beacon for homogeneous DNA detection. *Nanoscale* 2010, *2*, 1021–1026.

[62] Wu, C., Zhou, Y., Miao, X., Ling, L., A novel fluorescent biosensor for sequence-specific recognition of double-stranded DNA with the platform of graphene oxide. *Analyst* 2011, *136*, 2106–10.

[63] Guo, S., Du, D., Tang, L., Ning, Y., Yao, Q., Zhang, G.-J., PNA-assembled graphene oxide for sensitive and selective detection of DNA. *Analyst* 2013, *138*, 3216.

[64] Lee, J., Park, I.S., Jung, E., Lee, Y., Min, D.H., Direct, sequence-specific detection of dsDNA based on peptide nucleic acid and graphene oxide without requiring denaturation. *Biosens. Bioelectron.* 2014, *62*, 140–144.

[65] Liu, J., Fu, S., Yuan, B., Li, Y., Deng, Z., Toward a universal “adhesive nanosheet” for the assembly of multiple nanoparticles based on a protein-induced reduction/decoration of graphene oxide. *J. Am. Chem. Soc.* 2010, *132*, 7279–7281.

[66] Lee, J., Park, I.S., Kim, H., Woo, J.S., Choi, B.S., Min, D.H., BSA as additive: A simple strategy for practical applications of PNA in bioanalysis. *Biosens. Bioelectron.* 2015, *69*, 167–173.

[67] Wang, Y.H., Deng, H.H., Liu, Y.H., Shi, X.Q., Liu, A.L., Peng, H.P., Hong, G.L., Chen, W., Partially reduced graphene oxide as highly efficient DNA nanoprobe. *Biosens. Bioelectron.* 2016, *80*, 140–145.

[68] Dong, H., Zhang, J., Ju, H., Lu, H., Wang, S., Jin, S., Hao, K., Du, H., Zhang, X., Highly sensitive multiple microRNA detection based on fluorescence quenching of graphene oxide and isothermal strand-displacement polymerase reaction. *Anal. Chem.* 2012, *84*, 4587–4593.

[69] Hong, C., Baek, A., Hah, S.S., Jung, W., Kim, D.E., Fluorometric detection of microRNA using isothermal gene amplification and graphene oxide. *Anal. Chem.* 2016, *88*, 2999–3003.

[70] Tang, L., Wang, Y., Liu, Y., Li, J., DNA-directed self-assembly of

graphene oxide with applications to ultrasensitive oligonucleotide assay. *ACS Nano* 2011, *5*, 3817–3822.

[71]Li, C., Yang, Y., Zhang, B., Chen, G., Wang, Z., Li, G., Conjugation of graphene oxide with DNA-modified gold nanoparticles to develop a novel colorimetric sensing platform. *Part. Part. Syst. Charact.* 2014, *31*, 201–208.

[72] Haiss, W., Thanh, N.T.K., Aveyard, J., Fernig, D.G., Determination of size and concentration of gold nanoparticles from UV-Vis spectra. *Anal. Chem.* 2007, *79*, 4215–4221.